ZAMM · Z. Angew. Math. Mech. **90**, No. 7 – 8, 565 – 594 (2010) / **DOI** 10.1002/zamm.200900339

A pseudoelastic model for mechanical twinning on the microscale

R. Glüge[1,*], **A. Bertram**[1], **T. Böhlke**[2], **and E. Specht**[1]

[1] Otto-von-Guericke-Universität, Institut für Mechanik, Universitätsplatz 2, 39106 Magdeburg, Germany
[2] Karlsruhe Institut für Technologie (KIT), Institut für Technische Mechanik, Postfach 6980, 76128 Karlsruhe, Germany

Received 5 August 2009, revised 7 December 2009, accepted 29 January 2010
Published online 10 March 2010

Key words $\{10\bar{1}2\}\langle\bar{1}011\rangle$, twinning, pseudoelasticity, nonconvex strain energy, magnesium, crystal plasticity.

A pseudoelastic model for the simulation of deformation twinning on the microscale is developed and coupled with a crystal plasticity model for crystallographic slip. The material parameters are adopted to $\{10\bar{1}2\}\langle\bar{1}011\rangle$ twinning and basal glide in a magnesium alloy. Special attention is drawn to the energy invariance of conjugate twin systems that emerges when twinning is treated elastically. The model is tested in three characteristic FE simulations, namely a simple shear test parallel and inclined to a twin system and an elongation test of a notched band. The slip-twin interaction is studied, as well as the practical implications of the strain energy invariance. Some characteristics of twinning could be reproduced. The most important observations are that the load drop at the twin nucleation, the cusp shape of the twin tip in the absence of slip and the kink patterns that evolve in slip-twin interaction could be simulated.

1 Introduction

Deformation twinning is a major deformation mode encountered in many crystals. It is activated at low temperatures and high strain rates, i.e., when crystallographic slip is hindered. It is therefore able to extend the usability of many materials, which has been successfully demonstrated by the manganese alloyed TWIP (Twinning Induced Plasticity) steels. A crystal that undergoes twinning reorients its lattice, but unlike to martensitic transformations, does not change the lattice structure, which motivates the term "twinning". For shuffle-free twinning modes, the twin lattice is obtained by applying a homogeneous shear deformation to the parent lattice, while for twinning modes including shuffling, the homogeneous shear deformation leaves only the atoms of a sub-lattice in their proper twin configuration, while the remaining atoms undergo a shuffling displacement (Fig. 1). In both cases, a regular reordering of the atomic bonding is observed. Although from a chemical point of view one might not want to speak about a phase change, some characteristic ingredients of phase changes are encountered. Twinning produces sharp interfaces, at which the material properties that depend on the crystal orientation undergo a jump. The interfaces are approximately parallel to the shear plane. For classical twinning, the twin lattice is given by the mirroring the parent lattice in the shear plane (type 1 twinning), on the plane normal to the shear direction (type 2 twinning) (Christian [17]). If both orientation relations hold, one speaks of compound twins (Cahn [16]).

Twinning alters strongly the material properties, which is not always beneficial. The twins form plates inside of grains (Fig. 1), and can significantly alter the morphological and the crystallographic texture, both influencing the yield locus and the elastic anisotropy, while the additional interfaces have an impact on the strain hardening. Moreover, the twinning mechanism is polar, which can cause a pronounced differential effect on the strength of the material and on the forming limit, depending on the crystallographic texture. For many materials, these effects are not negligible. In particular, the ductile TWIP steels and the lightweight hcp metals, magnesium and titanium, which are interesting for engineering applications, show extensive twin formation at room temperature. Therefore, there is a need for the proper modeling of deformation twinning.

1.1 Classification into micro- and macromodels

In the context of the elasticity and plasticity of crystals, one usually refers to the microscale as the length scale of a single crystal, while on the marcoscale a representative number of crystals, i.e. a polycrystal, is covered. Similarly, one can classify micro- and macromodels into models which are designated to describe the behavior of a single crystal or a polycrystal, respectively. The most distinctive feature is that microscale models permit one specific crystal orientation at each material point, while macroscale models may account for crystal orientations by volume fractions which are assigned to specific orientations. One can therefore distinguish micro- and macromodels by asking whether stable phase mixtures

* Corresponding author E-mail: gluege@ovgu.de, Phone: +49 391 67 12592, Fax: +49 391 67 12863

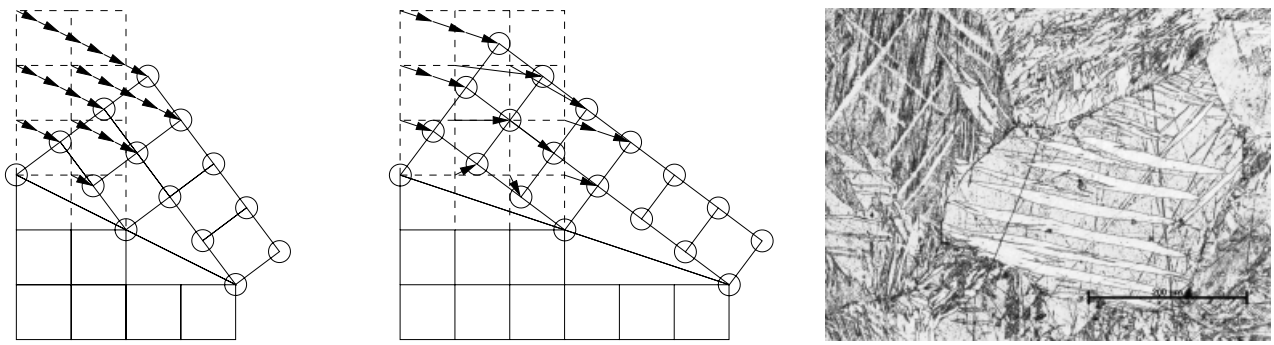

Fig. 1 Shuffle-free $\{012\}$ twinning (left) and shuffling-involving $\{013\}$ twinning (center) in a simple cubic lattice, micrograph of a magnesium polycrystal (right).

at one material point are permitted. From this distinction, the peculiarities of microscale modeling arise: one needs to deal with the phase transition in an erratic way, by tracking moving interfaces and taking into account the jumps that occur on the interface. On the macroscale, one needs to model the evolution of the volume fractions.

Both modeling scales have further advantages and drawbacks. The microscale modeling usually includes less material parameters than the macroscale modeling, which are of the single crystal, and physically meaningful. Moreover, it offers insight into interaction mechanisms between different phases. By taking into account automatically grain to grain interactions, it is to expect that microscale models are able to predict the macroscopic material behavior qualitatively better than macroscale models. On the other hand, macroscale results are only accessible by homogenization schemes, which are costly if carried out numerically, or need to be simplistic if carried out analytically (e.g. by Taylor's assumption).

In this work, a micromodel for twinning is proposed, and tested in different single-crystal simulations. In a consecutive work, the model will be tested in conjunction with the numerical homogenization scheme of deforming a representative volume element.

1.2 Pseudoelastic material behavior

Ericksen [21] argued that the characteristics of phase transitions can be described by elastic modeling with a nonconvex elastic strain energy. An illustrative example is the snap-spring, a connection of two springs, which has more than one stress-free configuration. Such snap-springs are employed by Müller [40], where the plastic material behavior is modeled with purely elastic constituents. Therefore, in continuum mechanics, such a modeling approach is considered as pseudoelastic. In material science, the term "pseudoelasticity" summarizes mechanically induced martensitic transformations, as observed by Bolling [14] and Lubenets [39], which enables large elastic, but not persistent deformations. In this work, we refer to "pseudoelasticity" in the sense of continuum mechanics.

By stating that each stable stress free configuration corresponds to a local minimum of the elastic strain energy, the latter cannot be convex. Applied to phase transitions, each local energy minimum is assigned to a different phase. Moreover, the phases are clearly separated by a nonconvex branch of the elastic strain energy, i.e., a unique assignment to a certain phase at each material point is given. The solution of the elastostatic boundary value problem is obtained by stating that the systems tends to its local energy-minimizing state, i.e., it is obtained by minimizing the free energy. Unfortunately, with a nonconvex elastic strain energy, the boundary value problem exhibits some unpleasant properties. Firstly, the existence of a unique solution is not ensured. Secondly, infinitely fine phase mixtures are predicted. Several remedies for the latter problems are proposed.

Convexification by construction of a convex hull. A fundamental work on convexity is given by Ball [9]. Given a nonconvex strain energy, it is reasonable to construct a convex hull, and to use the latter in place of the starting strain energy. Obviously, one looses the nonconvex branches of the strain energy. In this way, the uniqueness of the solution is gained at the cost of a clear assignment of the phases at each material point. Nevertheless, a volume fraction of each phase at each material point can be locally determined by introducing a dependence on the distance between the actual configuration and the stress free configurations of the phases. Talking about volume fractions, one has arrived at a macromodel. Sometimes, the construction of the convex hull is referred to as a relaxation procedure, since it corresponds to the relaxation of the constraint that at each material point only one phase exists. Some recently proposed relaxation procedures are given by Pagano [43], Lambrecht [36], Acerbi [2], Govindjee [25], Schmidt [48], and Peigney [45].

Convexification by incorporating higher-order strain gradients. By incorporating a contribution of a strain gradient to the elastic energy, one is able to penalize sharp strain gradients, which means that infinite fine phase mixtures are no more minimizers of the global strain energy. Physically, this comes close to the implementation of an interface energy, and is therefore referred to as a capillarity. The convexity of the strain energy is determined by the dependence on the highest strain gradient (Sidiamma [50]), i.e., one can regain the convexity. The use of higher-order strain gradients, however, has certain disadvantages. In reality, the deformations undergo a jump at an interface separating two phases. Therefore, the penalization of sharp strain gradients corresponds to a regularization of the jump at the interface. In order to obtain a reasonable approximation of the strain jump, the dependence of the strain energy on the strain gradient has to be strongly nonlinear. Moreover, the numerical treatment is more problematic, as well as the interpretation of the additional boundary conditions that have to be specified.

Kinetic relation. Instead of fixing the pseudoelastic modeling by constraining the strain energy density, one can interpret the deficiency of the model as a lack of physical considerations. Abeyaratne [1] states that the missing part is a nucleation criterion plus a kinetic relation. Haasen [29] stated similarly that phase mixtures are the result of kinetic processes, not of energy minimization alone. This has already been supposed by Gibbs, who assumed the existence of obstacles that prevent global energy minimization (Pego [44]). In fact, it is known that, e.g, the interface movement underlying to the twin propagation is controlled by the movement of partial dislocations, which has to be considered as a kinetic process.

By incorporating a kinetic relation, time-dependence enters into the considerations. One does not consider a global energy minimum anymore, but has to track an evolution. The ill-posedness of the pseudo-elastostatic boundary value problem is induced by oversimplifying the real material behavior. This becomes also clear by recognizing that the elastic modeling blanks out any evident strain-path dependence. The ill-posedness, as well as the missing strain-path dependence can be avoided by incorporating the underlying kinetic process.

1.3 Modeling outline

In this work, a nonconvex elastic energy density, denoted as compound strain energy $\tilde{w}$, is constructed, based on the assumption that the controlling strain energy is the one of the phase that has the least strain energy for a given deformation (Ball and James [7, 8]) (Sect. 2.1). This gives reasonable results near the stress-free configurations, but makes it necessary to further modify $\tilde{w}$ in the transition zones (Sect. 2.3). Then, the stress-strain law is derived by extending the elastic law that results from the compound strain energy by a linear viscous regularization, which serves as the kinetic relation (Sect. 2.4). Such an interface-independent kinetic relation has the advantage that one does not need to model the nucleation and the movement of the interfaces explicitly. The latter is not only very challenging from the practical point of view, but the laws of motion are unknown for most interfaces. They strongly depend on the phase propagation mechanism, which may be dominated by partial dislocation movement (as for $\{0\bar{1}11\}$ twinning in Mg, Li [38]) or by atomic shuffling (as for $\{0\bar{1}12\}$ twinning in Mg, Li [37]). Earlier implementations of similar modeling approaches are given by Silling [51], Swart [55], Collins [18], Klouček [34], Atai [6], Ortiz [42], and Wang [57]. In magnesium and its alloys, crystallographic slip is at room temperature restricted to the basal plane. Therefore, the visco-pseudoelastic material law is extended by the card glide mechanism, which enables the accommodation of slip in one plane (Sect. 2.5).

1.4 Notation

Throughout the work a direct tensor notation is preferred. If an expression cannot be represented in the direct notation without introducing new conventions, its components are given with respect to orthonormal base vectors $\boldsymbol{e}_i$, using the summation convention. Vectors are symbolized by lowercase bold letters $\boldsymbol{v} = v_i\boldsymbol{e}_i$, second-order tensors by uppercase bold letters $\boldsymbol{T} = T_{ij}\boldsymbol{e}_i \otimes \boldsymbol{e}_j$ or bold greek letters. The second-order identity tensor is denoted by $\boldsymbol{I}$. Fourth-order tensors are symbolized like $\mathbb{C}$. The dyadic product is defined as $(\boldsymbol{a} \otimes \boldsymbol{b}) \cdot \boldsymbol{c} = (\boldsymbol{b} \cdot \boldsymbol{c})\boldsymbol{a}$. Matrices are denoted like $[A]$. A dot represents a scalar contraction. If more than one scalar contraction is carried out, the number of dots corresponds to the number of vectors that are contracted, thus $\boldsymbol{a} \otimes \boldsymbol{b} \otimes \boldsymbol{c} \cdot\cdot\, \boldsymbol{d} \otimes \boldsymbol{e} = (\boldsymbol{b} \cdot \boldsymbol{d})(\boldsymbol{c} \cdot \boldsymbol{e})\boldsymbol{a}$, $\boldsymbol{v} = \boldsymbol{A} \cdot \boldsymbol{w}$, $\alpha = \boldsymbol{A} \cdot\cdot\, \boldsymbol{B}$ and $\boldsymbol{\sigma} = \mathbb{C} \cdot\cdot\, \boldsymbol{\varepsilon}$. When only one scalar contraction is carried out, the scalar dot is frequently omitted, e.g., $\boldsymbol{v} = \boldsymbol{F}\boldsymbol{w}$, $\boldsymbol{A} = \boldsymbol{B}\boldsymbol{C}$. The Rayleigh-product is defined by applying a second-order tensor to the base vectors of a tensor. E.g., in case of a fourth-order tensor, $\boldsymbol{P} * \mathbb{C} = C_{ijkl}\boldsymbol{P}\boldsymbol{e}_i \otimes \boldsymbol{P}\boldsymbol{e}_j \otimes \boldsymbol{P}\boldsymbol{e}_k \otimes \boldsymbol{P}\boldsymbol{e}_l$, with $\mathbb{C} = C_{ijkl}\boldsymbol{e}_i \otimes \boldsymbol{e}_j \otimes \boldsymbol{e}_k \otimes \boldsymbol{e}_l$. Orthogonal tensors are denoted by $\boldsymbol{Q}_{\beta\boldsymbol{v}} = \tilde{\boldsymbol{e}}_i \otimes \boldsymbol{e}_i$, mapping one orthonormal basis $\boldsymbol{e}_i$ into another one $\tilde{\boldsymbol{e}}_i$. If $\boldsymbol{Q}$ can be interpreted as a rotation, the optional indexing contains the amount of rotation β and the normalized axial vector $\boldsymbol{v}$. Two-fold rotations are rotations of amount π. They are denoted as $\boldsymbol{R}_{\boldsymbol{v}} = -\boldsymbol{I} + 2\boldsymbol{v} \otimes \boldsymbol{v}$, with $\boldsymbol{v}$ being the normalized axial vector. The derivative of a vector valued vector function with respect to its argument is denoted like $\boldsymbol{v}'(\boldsymbol{w}) = \partial\boldsymbol{v}(\boldsymbol{w})/\partial\boldsymbol{w} = \partial v_i/\partial w_j \;\; \boldsymbol{e}_i \otimes \boldsymbol{e}_j$. The material time derivative is indicated by a dot, placed above the function under consideration.

1.5 The hexagonal lattice

For a hexagonal lattice, it is convenient to use the Miller-Bravais basis

$$\boldsymbol{a}_1 = a\boldsymbol{e}_1, \tag{1}$$

$$\boldsymbol{a}_2 = a\left(-\frac{1}{2}\boldsymbol{e}_1 + \frac{\sqrt{3}}{2}\boldsymbol{e}_2\right), \tag{2}$$

$$\boldsymbol{a}_3 = a\left(-\frac{1}{2}\boldsymbol{e}_1 - \frac{\sqrt{3}}{2}\boldsymbol{e}_2\right), \tag{3}$$

$$\boldsymbol{c} = c\boldsymbol{e}_3, \tag{4}$$

see Fig. 2, (Neumann, [41], Pitteri [46]). The lattice parameters c and a represent the height of the cell and the edge length of the base hexagon, respectively, and correspond to the norms of $\boldsymbol{c}$ and $\boldsymbol{a}$, $c = \sqrt{\boldsymbol{c}\cdot\boldsymbol{c}}$ and $a = \sqrt{\boldsymbol{a}\cdot\boldsymbol{a}}$. Although one usually does not appreciate the use of linearly dependent base vectors, this basis has the advantage that it reflects the hexagonal symmetry. Permutations of the components belonging to $\boldsymbol{a}_{1\ldots3}$, a change of sign of the c-component or a simultaneous change of sign of all $a_{1\ldots3}$ yield crystallographically equivalent directions, which are denoted as $\langle a_1 a_2 a_3 c\rangle$. Usually, negative components are denoted by $\bar{x}$ instead of $-x$. Further, due to the linear dependence of $\boldsymbol{a}_{1\ldots3}$, the condition $a_1 + a_2 + a_3 = 0$ is imposed, and therefore sometimes the third component a_3 is omitted.
To indicate planes, it is advantageous to introduce another basis. This is done by taking the dual basis $(\tilde{\boldsymbol{a}}_1, \tilde{\boldsymbol{a}}_2, \tilde{\boldsymbol{c}})$ of $(\boldsymbol{a}_1, \boldsymbol{a}_2, \boldsymbol{c})$ and defining the base vectors

$$\boldsymbol{a}_1^* = \frac{2}{3}\tilde{\boldsymbol{a}}_1 - \frac{1}{3}\tilde{\boldsymbol{a}}_2 = \frac{2}{3a^2}\boldsymbol{a}_1, \tag{5}$$

$$\boldsymbol{a}_2^* = -\frac{1}{3}\tilde{\boldsymbol{a}}_1 + \frac{2}{3}\tilde{\boldsymbol{a}}_2 = \frac{2}{3a^2}\boldsymbol{a}_2, \tag{6}$$

$$\boldsymbol{a}_3^* = -\frac{1}{3}\tilde{\boldsymbol{a}}_1 - \frac{1}{3}\tilde{\boldsymbol{a}}_2 = \frac{2}{3a^2}\boldsymbol{a}_3, \tag{7}$$

$$\boldsymbol{c}^* = \tilde{\boldsymbol{c}} = \frac{1}{c^2}\boldsymbol{c}. \tag{8}$$

This basis again satisfies $\boldsymbol{a}_1^* + \boldsymbol{a}_2^* + \boldsymbol{a}_3^* = 0$, but it is not the dual basis of $(\boldsymbol{a}_1, \boldsymbol{a}_2, \boldsymbol{a}_3, \boldsymbol{c})$. It also has the advantage that crystallographically equivalent planes are connected by permutations of the components and changes of sign as stated above. Again, the components should be restricted to $a_1^* + a_2^* + a_3^* = 0$. If this is done, several practical simplifications are obtained: If a normal vector is given with respect to the basis $(\boldsymbol{a}_1^*, \boldsymbol{a}_2^*, \boldsymbol{a}_3^*, \boldsymbol{c}^*)$, the reciprocals of its components correspond to the piercing point distances of the plane with the base vectors $(\boldsymbol{a}_1, \boldsymbol{a}_2, \boldsymbol{a}_3, \boldsymbol{c})$. Therefore, the plane $\{10\bar{1}2\}$ can be visualized by considering the points $\boldsymbol{a}_1$, $-\boldsymbol{a}_3$ and $1/2\boldsymbol{c}$ (see Fig. 2). Moreover, one can easily see whether direction and normal vectors are perpendicular to each other by calculating the scalar product as if $(\boldsymbol{a}_1, \boldsymbol{a}_2, \boldsymbol{a}_3, \boldsymbol{c})$ and $(\boldsymbol{a}_1^*, \boldsymbol{a}_2^*, \boldsymbol{a}_3^*, \boldsymbol{c}^*)$ were dual bases. One notes easily that $\langle 10\bar{1}1\rangle$ and $\{\bar{1}012\}$ are perpendicular to each other:

$$(\boldsymbol{a}_1 - \boldsymbol{a}_3 + \boldsymbol{c})\cdot(-\boldsymbol{a}_1^* + \boldsymbol{a}_3^* + 2\boldsymbol{c}^*) = -\boldsymbol{a}_1\cdot\boldsymbol{a}_1^* + \boldsymbol{a}_1\cdot\boldsymbol{a}_3^* - \boldsymbol{a}_3\cdot\boldsymbol{a}_3^* + \boldsymbol{a}_3\cdot\boldsymbol{a}_1^* + 2\boldsymbol{c}\cdot\boldsymbol{c}^* \tag{9}$$

$$= -\frac{2}{3} - \frac{1}{3} - \frac{2}{3} - \frac{1}{3} + 2 = 0. \tag{10}$$

2 Model derivation

2.1 Construction of a global elastic energy

Following Ball and James [7, 8], the elastic energy of a material that can form n different phases is given by

$$w(\boldsymbol{E}) = \min_{i=1\ldots n}(w_1(\boldsymbol{E}), w_2(\boldsymbol{E}), \ldots w_n(\boldsymbol{E})), \tag{11}$$

with w_i being the individual elastic energies of the phases. This algebraic assignment is evaluated pointwise. The strain energies depend only on the strains $\boldsymbol{E}$, which is omitted in the remainder of this section. In order to derive an elastic law,

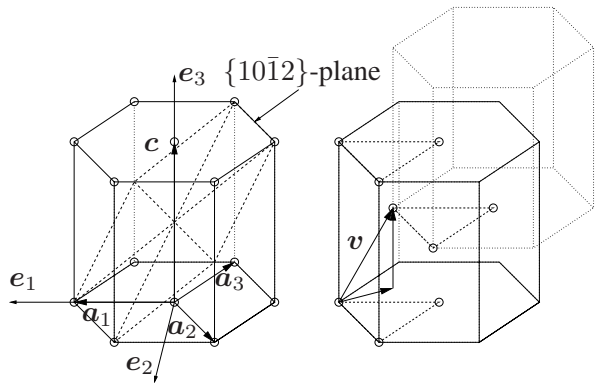

Fig. 2 Simple hexagonal lattice with Miller-Bravais basis (left), hexagonal close packed multilattice constructed from the simple lattice by introducing additional translations in $\boldsymbol{v} = \langle \frac{\bar{1}}{3} 0 \frac{1}{3} \frac{1}{2} \rangle$ (right).

the derivative of w with respect to the strains is needed. Therefore, a regularization $\tilde{w}$ to replace Eq. (11) is constructed. It should contain a regularization parameter, say k, so that the limit becomes

$$\lim_{k \to \infty} \tilde{w} = w. \tag{12}$$

The w_i represent the elastic strain energies, which means that $w_i = 0$ in the stress-free states, and $w_i \geq 0$ holds. As a starting point, the pointwise addition

$$\tilde{w} = \sum_{i=1}^{n} a_i(w_1, w_2, \ldots w_n) w_i \tag{13}$$

is made, where the a_i are weight factors. In the limit case (Eq. 12), the weight factor a_m of the smallest w_m should approach 1, while all the other a_i should tend to zero. Therefore the normalization

$$\sum_{i=1}^{n} a_i(w_1, w_2, \ldots w_n) = 1 \tag{14}$$

is imposed. It is obtained by

$$a_i(g_1, g_2, \ldots g_n) = \frac{g_i(w_1, w_2, \ldots w_n)}{\sum_{j=1}^{n} g_j(w_1, w_2, \ldots w_n)}, \tag{15}$$

where now $g_i(w_1, w_2, \ldots w_n)$ has to be specified. The location of the minima of the individual w_i should be transferred to $\tilde{w}$ independently of k. This restriction is imposed in order to not alter the location of the stress free configurations by the choice of k. As the minimum of the individual strain energies w_i is equal to zero, the $g_i(w_1, w_2, \ldots w_n)$ should be constructed such that all $g_i(w_1, w_2, \ldots w_n) = 0$ and $g_m(w_1, w_2, \ldots w_n) > 0$ when $w_m = 0,\ i = 1 \ldots n, i \neq m$. This results in vanishing $g_i(w_1, w_2, \ldots w_n)$ except the one $g_m(w_1, w_2, \ldots w_n)$ corresponding to the vanishing energy density w_m. The imposed restrictions are met by

$$g_i(w_1, w_2, \ldots w_n) = h_i(w_i) \prod_{j=1}^{n, j \neq i} (1 - h_j(w_j)) = \frac{h_i(w_i)}{1 - h_i(w_i)} \prod_{j=1}^{n} (1 - h_j(w_j)) \tag{16}$$

with

$$h(w = 0) = 1, \qquad h(w \to \infty) = 0. \tag{17}$$

By this constraint, the minima of the w_i are transferred to $\tilde{w}$ independently of the regularization parameter k, as long as the minimum corresponds to a zero energy density. The constraints imposed on $h(w)$ are met, e.g., by

$$h(w) = \exp(-kw). \tag{18}$$

By inserting the deduced $g_i(w_1, w_2, \ldots w_n)$ into the $a_i(g_1, g_2, \ldots g_n)$, one sees that the product term is canceled out, i.e., it suffices to take

$$g_i = \frac{h(w_i)}{1 - h(w_i)}. \tag{19}$$

Finally, the regularized strain energy

$$\tilde{w} = \left(\sum_{j=1}^{n} \frac{h(w_j)}{1-h(w_j)} \right)^{-1} \sum_{i=1}^{n} \frac{h(w_i)}{1-h(w_i)} w_i, \qquad h(w) = \exp(-kw) \tag{20}$$

is obtained. The given approach is visualized for testfunctions in Fig. 3. In the remainder of this section it is shown that the regularization approaches the Ball and James-approach from above if $k \to \infty$. For facility of inspection, the chain-like dependency of $a_i(g_1, g_2 \dots g_n)$, $g_i(w_i)$ is omitted.

Subtracting pointwise the smallest w_m out of the w_i from $\tilde{w}$ gives a remainder $\delta = \tilde{w} - w_m$, which should vanish for $k \to \infty$:

$$\delta = \sum_{i=1}^{n} a_i w_i - w_m, \qquad w_m = \min_{i=1\dots n} (w_1, w_2, \dots w_n). \tag{21}$$

All w_i can be written as w_m plus some positive difference Δw_i

$$\delta = \sum_{i=1}^{n} a_i (w_m + \Delta w_i) - w_m. \tag{22}$$

With $\sum_{i=1}^{n} a_i = 1$ one finds

$$\delta = \sum_{i=1}^{n, i \neq m} a_i \Delta w_i, \tag{23}$$

which is positive due to $a_i \geq 0$ and $\Delta w_i \geq 0$. This means that $\tilde{w} \geq w$, i.e. the regularization approaches the Ball and James-approach from above. To show that δ tends to zero for $k \to \infty$, the latter equation is divided by a_m, which corresponds to the weight factor of w_m:

$$\frac{\delta}{a_m} = \sum_{i=1}^{n, i \neq m} \frac{a_i}{a_m} \Delta w_i \ . \tag{24}$$

Calculating the limit $k \to \infty$ of the a_i/a_m yields

$$\lim_{k\to\infty} \frac{a_i}{a_m} = \lim_{k\to\infty} \frac{g_i}{g_m} \tag{25}$$

$$= \lim_{k\to\infty} \frac{h(w_i)(1-h(w_m))}{h(w_m)(1-h(w_i))} \tag{26}$$

$$= \lim_{k\to\infty} \frac{h(w_i)}{h(w_m)} \lim_{k\to\infty} \frac{1-h(w_m)}{1-h(w_i)}. \tag{27}$$

Due to $\lim_{k\to\infty} h = 0$ the limit (27) is obtained by

$$\lim_{k\to\infty} \frac{a_i}{a_m} = \lim_{k\to\infty} \frac{h(w_i)}{h(w_m)} \tag{28}$$

$$= \lim_{k\to\infty} \exp(-k(w_i - w_m)), \tag{29}$$

which yields 0 for $w_i > w_m,\ i \neq m$, which in fact was our initial assumption. We are left with

$$\lim_{k\to\infty} \frac{\delta}{a_m} = 0. \tag{30}$$

Due to $\sum_{i=1}^{n} a_i = 1$ and $\lim_{k\to\infty} (a_i/a_m) = 0$ for $i \neq m$, $a_m = 1$ must hold, which finally yields

$$\lim_{k\to\infty} \delta = 0 \quad \Leftrightarrow \quad \lim_{k\to\infty} \tilde{w} = \min_{i=1\dots n} (w_1, w_2, \dots w_n). \tag{31}$$

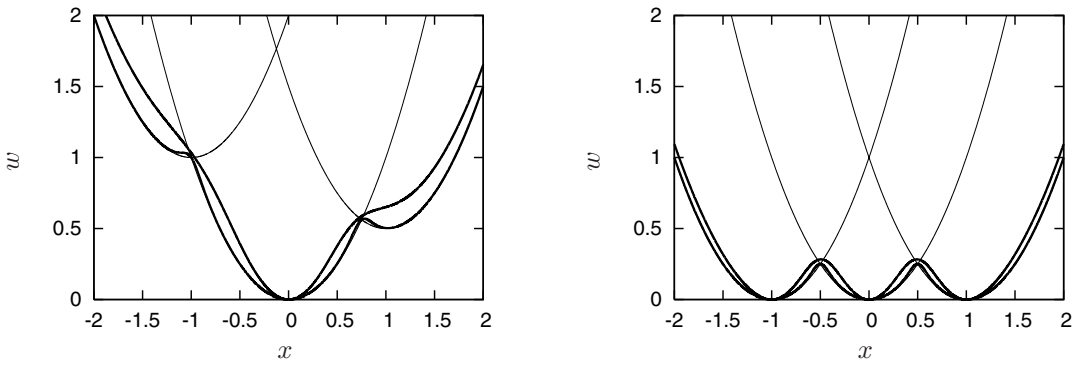

Fig. 3 Regularization (bold lines) applied to $w_1 = x^2$, $w_2 = (x-1)^2 + 0.5$, $w_3 = w_2 = (x+1)^2 + 1$ (left) and $w_1 = x^2$, $w_2 = (x-1)^2$, $w_3 = (x+1)^2$ (right), with $k = 1$ and $k = 10$. In the second case, as all w_i have zero as minimum, the regularization transfers the minima of the w_i to w independently on k.

2.2 The individual strain energies

Now that a regularization of Eq. (11) is given, we focus on the individual strain energies w_i. The widely used principle of Euclidean invariance demands that the strain energy density w_i depends only on the material stretching, but not on a superimposed rigid body motion. Consequently, it is sufficient to note $w_i(\boldsymbol{C})$ instead of $w_i(\boldsymbol{F})$ (Truesdell [56]), with $\boldsymbol{C} = \boldsymbol{F}^T\boldsymbol{F}$ and the deformation gradient $\boldsymbol{F}$. The elastic material behavior of most crystals can be described sufficiently well by a linear stress-strain relation. Therefore, the St. Venant-Kirchhoff strain energy will be employed here. The elastic reference strain energy is given by

$$w_0(\boldsymbol{C}) = \frac{1}{2}\boldsymbol{T} \cdot\cdot\, \boldsymbol{E} \tag{32}$$

$$= \frac{1}{8}(\boldsymbol{C} - \boldsymbol{I}) \cdot\cdot\, \mathbb{C}_0 \cdot\cdot\, (\boldsymbol{C} - \boldsymbol{I}), \tag{33}$$

with the stiffness tetrad $\mathbb{C}_0$. The second Piola-Kirchhoff stresses $\boldsymbol{T}$ and Green's strains $\boldsymbol{E} = \frac{1}{2}(\boldsymbol{C} - \boldsymbol{I})$ are work-conjugate, which simplifies the formulation of w_0 and its derivatives with respect to $\boldsymbol{E}$ (Hill [30]).

Due to the fact that the twinned crystal has the same crystallographic structure as the parent crystal, the same elastic energy is applicable. Therefore, the concept of elastic isomorphisms (Bertram [11]) is used in order to map the elastic reference energy (33) to the parent and to the twin. Since the elastic isomorphisms are mostly connected to a change of the stress-free configuration, which is usually considered as a plastic deformation, they are also referred to as plastic transformations. By using the isomorphisms $\boldsymbol{P}_i$, the elastic energy can be transformed by

$$w_i(\boldsymbol{C}) = w_0(\boldsymbol{P}_i^T\boldsymbol{C}\boldsymbol{P}_i) \tag{34}$$

to the elastic energy of the ith twin variant, where $\boldsymbol{P}_i$ maps lattice reference basis $\boldsymbol{c}_b$ into the reference placement of the parent or the ith twin variant. The second Piola-Kirchhoff-stresses are given by

$$\boldsymbol{T}_i = \frac{\partial w_i}{\partial \boldsymbol{E}} \tag{35}$$

$$= 2\frac{\partial w_i}{\partial \boldsymbol{C}} \tag{36}$$

$$= 2\frac{\partial w_0(\boldsymbol{P}_i^T\boldsymbol{C}\boldsymbol{P}_i)}{\partial(\boldsymbol{P}_i^T\boldsymbol{C}\boldsymbol{P}_i)} \cdot\cdot\, \frac{\partial \boldsymbol{P}_i^T\boldsymbol{C}\boldsymbol{P}_i}{\partial \boldsymbol{C}} \tag{37}$$

$$= 2\boldsymbol{P}_i w_0'(\boldsymbol{P}_i^T\boldsymbol{C}\boldsymbol{P}_i)\boldsymbol{P}_i^T. \tag{38}$$

In the following, the needed isomorphisms are derived.

$\boldsymbol{P}_P$ and $\boldsymbol{P}_T$ map the reference lattice basis $\boldsymbol{c}_b$ to the reference placement, i.e. either to the parent ($\boldsymbol{c}_{Pb}$) or the twin ($\boldsymbol{c}_{Tb}$),

$$\boldsymbol{c}_{Pb} = \boldsymbol{P}_P\boldsymbol{c}_b, \tag{39}$$

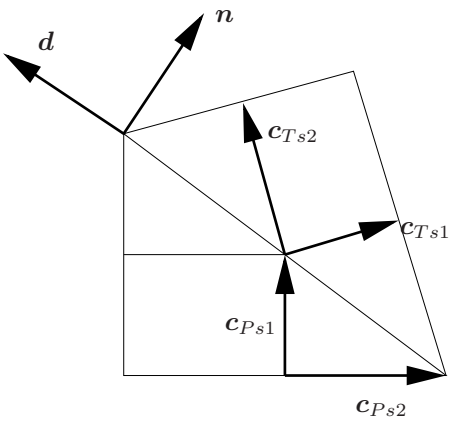

Fig. 4 In the spatial description, the lattice vectors of parent and twin differ by a rotation of π around $\boldsymbol{n}$. The associated deformation is a simple shear deformation.

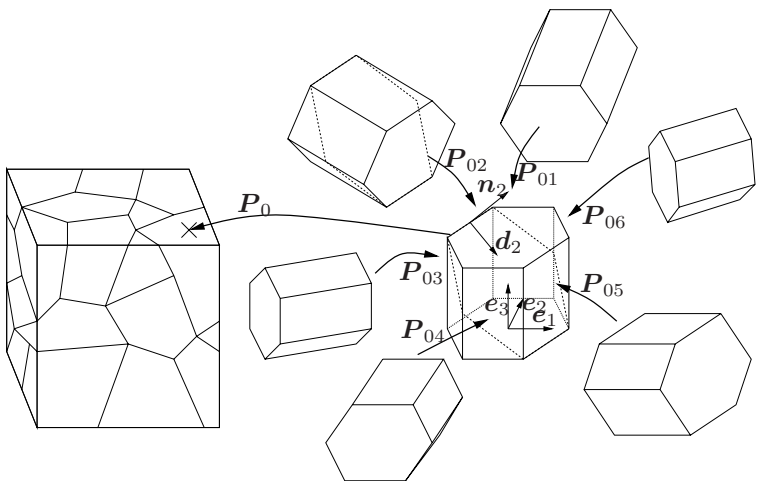

Fig. 5 Connection of elastic reference law and reference placement for a schematic representative volume element.

$$\boldsymbol{c}_{Tb} = \boldsymbol{P}_T \boldsymbol{c}_b. \tag{40}$$

The spatial lattice base vectors $\boldsymbol{c}_{Ps}$ and $\boldsymbol{c}_{Ts}$ are given by the deformation gradients $\boldsymbol{F}_P$ and $\boldsymbol{F}_T$,

$$\boldsymbol{c}_{Ps} = \boldsymbol{F}_P \boldsymbol{c}_{Pb}, \tag{41}$$

$$\boldsymbol{c}_{Ts} = \boldsymbol{F}_T \boldsymbol{c}_{Tb}. \tag{42}$$

$\boldsymbol{c}_{Ps}$ and $\boldsymbol{c}_{Ts}$ are related by the reorientation $\boldsymbol{R}$ of the lattice,

$$\boldsymbol{c}_{Ts} = \boldsymbol{R} \boldsymbol{c}_{Ps}. \tag{43}$$

Now one can evaluate $\boldsymbol{P}_T$ by means of

$$\boldsymbol{P}_T \boldsymbol{c}_b = \boldsymbol{c}_{Tb} = \boldsymbol{F}_T^{-1} \boldsymbol{c}_{Ts} = \boldsymbol{F}_T^{-1} \boldsymbol{R} \boldsymbol{c}_{Ps} = \boldsymbol{F}_T^{-1} \boldsymbol{R} \boldsymbol{F}_P \boldsymbol{c}_{Pb} = \boldsymbol{F}_T^{-1} \boldsymbol{R} \boldsymbol{F}_P \boldsymbol{P}_P \boldsymbol{c}_b \tag{44}$$

which allows for the identification

$$\boldsymbol{P}_T = \boldsymbol{F}_T^{-1} \boldsymbol{R} \boldsymbol{F}_P \boldsymbol{P}_P. \tag{45}$$

By taking the elastic law of the parent to be the reference law, and the placement of the parent to be the reference placement, i.e. $\boldsymbol{P}_P = \boldsymbol{I},\ \boldsymbol{F}_P = \boldsymbol{I}$, Eq. (45) simplifies to

$$\boldsymbol{P}_T = \boldsymbol{F}_T^{-1} \boldsymbol{R}. \tag{46}$$

$\boldsymbol{R}$ denotes the reorientation of the lattice. It is $\boldsymbol{R}_{\boldsymbol{n}}$ for type 1 twinning and $\boldsymbol{R}_{\boldsymbol{d}}$ for type 2 twinning. In case of a compound twin, both orientation relations hold (Cahn, [16]). $\boldsymbol{F}_T$ describes the deformation from the parent to the twin configuration, which is given by a simple shear deformation

$$\boldsymbol{F}_T = \boldsymbol{I} + \gamma_0 \boldsymbol{d} \otimes \boldsymbol{n}. \tag{47}$$

Due to the orthogonality of $\boldsymbol{d}$ and $\boldsymbol{n}$ its inverse is given by $\boldsymbol{F}_T^{-1} = \boldsymbol{I} - \gamma_0 \boldsymbol{d} \otimes \boldsymbol{n}$, which finally yields

$$\boldsymbol{P}_T = (\boldsymbol{I} - \gamma_0 \boldsymbol{d} \otimes \boldsymbol{n})(-\boldsymbol{I} + 2\boldsymbol{n} \otimes \boldsymbol{n}) \tag{48}$$

$$= -\boldsymbol{I} - \gamma_0 \boldsymbol{d} \otimes \boldsymbol{n} + 2\boldsymbol{n} \otimes \boldsymbol{n} \tag{49}$$

in the case of $\boldsymbol{R} = \boldsymbol{R}_{\boldsymbol{n}}$ and

$$\boldsymbol{P}_{T(\boldsymbol{d})} = (\boldsymbol{I} - \gamma_0 \boldsymbol{d} \otimes \boldsymbol{n})(-\boldsymbol{I} + 2\boldsymbol{d} \otimes \boldsymbol{d}) \tag{50}$$

$$= -\boldsymbol{I} + \gamma_0 \boldsymbol{d} \otimes \boldsymbol{n} + 2\boldsymbol{d} \otimes \boldsymbol{d} \tag{51}$$

in the case of $\boldsymbol{R} = \boldsymbol{R}_{\boldsymbol{d}}$. Note that, in both cases, $\boldsymbol{P}_T$ has the remarkable property of self-inverseness, $\boldsymbol{P}_T = \boldsymbol{P}_T^{-1}$. Therefore, double twinning on the same twin system results in a recovery of the parent.

2.3 Phenomenological model adaption

Following the Ball and James approach, the determining strain energy density w_i is the smallest one. Consequently, if a monotonic strain driven test from the stress free parent to the stress free twin configuration is carried out, the transition point is halfway between the two stress free states, due to the isomorphic elastic laws. Therefore, the shear stress in the twin system before the transition can be estimated by $\tau \approx G\gamma_0/2$, with the apparent shear modulus G in the twin system. For $\{10\bar{1}2\}\langle\bar{1}011\rangle$ twinning in magnesium, one obtains $\tau \approx 17000\,\mathrm{MPa} \times 0.13/2 \approx 1100\,\mathrm{MPa}$. This twinning stress is orders of magnitude too large. The reason for the drastic overestimation is the disregard of the twin propagation mechanism, namely the movement of partial dislocations. The latter provides the kinetic relation that completes the pseudoelastic approach in a natural way. It would now be necessary to include a nucleation criterion and a kinetic relation. However, here, a more simple track is followed. The stresses obtained from the elastic law are bounded, while the time dependence enters by the viscous regularization.

Adaption of the elastic law. With the w_i on hand, one can derive

$$\boldsymbol{T} = \frac{\partial w_i}{\partial \boldsymbol{E}}, \tag{52}$$

and restrict the stresses to admissible stress states by using a projection method. In doing so, one violates in general the integrability conditions for a hyperelastic stress strain relation. Therefore, instead of adapting $\boldsymbol{T}$, the model adaption is transferred to w. In this way the existence of the strain energy is ensured.

For the explanation of the concept, the indexing of the different phases and the configuration change are omitted in this section. As the individual strain energies are defined in terms of strains, an indicator function $\phi(\boldsymbol{E})$ is defined, which is used to identify critical strain states, beyond which the strain energy is modified. If $\phi(\boldsymbol{E}) < 0$, $\boldsymbol{E}$ is a subcritical strain state. If $\phi(\boldsymbol{E}) > 0$, $\boldsymbol{E}$ is an overcritical strain state. The critical strain states correspond to $\phi(\boldsymbol{E}) = 0$. A critical strain state connected to an overcritical strain $\boldsymbol{E}$ can be specified by an orthogonal projection

$$\boldsymbol{E}_{\mathrm{crit}} = \boldsymbol{E} - \lambda\phi'(\boldsymbol{E}_{\mathrm{crit}}), \qquad \phi(\boldsymbol{E}_{\mathrm{crit}}) = 0, \tag{53}$$

sketched in Fig. 6. Alternatively, one could think of a critical strain state assignment $\boldsymbol{E}_{\mathrm{crit}}(\boldsymbol{E})$ by demanding $\min\|\boldsymbol{E} - \boldsymbol{E}_{\mathrm{crit}}\|,\ \phi(\boldsymbol{E}_{\mathrm{crit}}) = 0$. The latter formulation is alike the projection method, but it does not depend on the $\mathcal{C}^1$ continuity of $\phi(\boldsymbol{E})$. An even simpler approach is the radial return method $\boldsymbol{E}_{\mathrm{crit}} = \alpha\boldsymbol{E},\ \phi(\boldsymbol{E}_{\mathrm{crit}}) = 0$, which does not even need the convexity of $\phi(\boldsymbol{E})$. In anticipation of the numerical results, no significant difference between the orthogonal projection and the radial return method could be determined.

Focusing on the definition of ϕ, if a critical twinning shear strain γ_{twin} is defined in one potential twin system, one can take

$$\phi_1(\boldsymbol{E}) = \gamma - \gamma_{\mathrm{twin}}, \qquad \gamma = 2\boldsymbol{E}\cdot\cdot\boldsymbol{M}, \qquad \boldsymbol{M} = \boldsymbol{d}\otimes\boldsymbol{n}. \tag{54}$$

For this simple case, Eq. (53) can be solved explicitly for $\boldsymbol{E}_{\mathrm{crit}}$, namely

$$\boldsymbol{E}_{\mathrm{crit}} = \boldsymbol{E} - \lambda\mathrm{sym}(\boldsymbol{M}), \qquad \lambda = \gamma - \gamma_{\mathrm{twin}}. \tag{55}$$

The latter projection is useful if only one twin system is potentially active. If more than one twin system can be activated, the "critical strain state hypersurface" has to be constructed such that a unique assignment $\boldsymbol{E} \to \boldsymbol{E}_{\mathrm{crit}}$ is possible. I.e., it must be $\mathcal{C}^1$ continuous and convex in the sense that $\phi(\alpha\boldsymbol{E}_{\mathrm{crit1}} + (1-\alpha)\boldsymbol{E}_{\mathrm{crit2}}) < 0,\ \alpha \in [0,1]$ holds for any two critical strain states. Moreover, a "shooting through" the domain of admissible strain states is always possible, which yields two solutions for $\boldsymbol{E}_{\mathrm{crit}}$. The feasible one is the one which is closer to the strain state $\boldsymbol{E}$, i.e., the one with the smaller absolute value of λ.

A possible ϕ_n for n different twin systems is

$$\phi_n(\boldsymbol{E}) = \sum_{i=1}^{n}\langle\gamma_i/\gamma_{\mathrm{twin}}\rangle^m - 1, \qquad \gamma_i = 2\boldsymbol{E}\cdot\cdot\boldsymbol{M}_i, \tag{56}$$

with $\langle x\rangle = (x + |x|)/2$ to respect the polarity of twinning. Here, if one out of the n distinct $\gamma_i > \gamma_{\mathrm{twin}}$, then $\phi_n(\boldsymbol{E}) > 0$. m is a preferably large integer regularization parameter. By taking a large value for m, γ_{twin} can practically be reached in all twin systems simultaneously without passing a critical strain state. For $m > 1$, $\boldsymbol{E}_{\mathrm{crit}}$ cannot be given explicitly.

With the critical strain definition on hand, one is able to modify the strain energy. It is pointed out again that beyond the critical strain state, the strain energy density is used as a pure modeling tool, but its existence in the large assures the thermodynamic consistency. The following modified strain energy is applied:

$$w = w_0 = \frac{1}{2}\boldsymbol{E}\cdot\cdot\,\mathbb{C}\cdot\cdot\,\boldsymbol{E} \quad \text{if} \quad \phi(\boldsymbol{E}) \leq 0, \tag{57}$$

$$w = w_0 - \frac{1}{2}(\boldsymbol{E}-\boldsymbol{E}_{\mathrm{crit}})\cdot\cdot\,\mathbb{C}_0\cdot\cdot\,(\boldsymbol{E}-\boldsymbol{E}_{\mathrm{crit}}) \quad \text{if} \quad \phi(\boldsymbol{E}) > 0. \tag{58}$$

One notes that with the index symmetries of $\mathbb{C}_0$, in the case of $\phi(\boldsymbol{E}) > 0$, w can be simplified to

$$w = \boldsymbol{E}\cdot\cdot\,\mathbb{C}_0\cdot\cdot\boldsymbol{E}_{\mathrm{crit}} - \frac{1}{2}\boldsymbol{E}_{\mathrm{crit}}\cdot\cdot\,\mathbb{C}_0\cdot\cdot\,\boldsymbol{E}_{\mathrm{crit}}. \tag{59}$$

The latter modification of w is chosen because it is $\mathcal{C}^1$ continuous. Moreover, it ensures that the stress level does not increase past the critical strain state. If we ignore the dependence of $\boldsymbol{E}_{\mathrm{crit}}$ on $\boldsymbol{E}$, we yield a strain energy which is linear in $\boldsymbol{E}$. In a monotonic strain driven test (in direction of $\partial\phi/\partial\boldsymbol{E}|_{\boldsymbol{E}_{\mathrm{crit}}}$, i.e. $\boldsymbol{E}_{\mathrm{crit}}$ is constant), one obtains a constant stress strain relation beyond the critical strain state, corresponding to the linear increase of w.

To calculate the stresses $\boldsymbol{T} = \partial w/\partial\boldsymbol{E}$, the derivative $\partial\boldsymbol{E}_{\mathrm{crit}}/\partial\boldsymbol{E}$ is needed. $\boldsymbol{E}_{\mathrm{crit}}$ is given implicitly by Eq. (53), which can be rearranged as

$$\mathbf{0} = \boldsymbol{g} = \boldsymbol{E} - \lambda\phi'(\boldsymbol{E}_{\mathrm{crit}}) - \boldsymbol{E}_{\mathrm{crit}} \tag{60}$$

$$0 = g = \phi(\boldsymbol{E}_{\mathrm{crit}}). \tag{61}$$

The dependence of ϕ and its derivatives on $\boldsymbol{E}_{\mathrm{crit}}$ is omitted in the remainder. The complete differential of the latter equations with respect to $\boldsymbol{E}$ is also zero, so that

$$\mathbf{0} = \frac{\mathrm{d}\boldsymbol{g}}{\mathrm{d}\boldsymbol{E}} = \mathbb{I}^S - \lambda\phi''\cdot\cdot\,\frac{\partial\boldsymbol{E}_{\mathrm{crit}}}{\partial\boldsymbol{E}} - \phi'\otimes\frac{\partial\lambda}{\partial\boldsymbol{E}} - \frac{\partial\boldsymbol{E}_{\mathrm{crit}}}{\partial\boldsymbol{E}} \tag{62}$$

$$= \mathbb{I}^S - \phi'\otimes\frac{\partial\lambda}{\partial\boldsymbol{E}} - (\lambda\phi'' + \mathbb{I}^S)\cdot\cdot\,\frac{\partial\boldsymbol{E}_{\mathrm{crit}}}{\partial\boldsymbol{E}} \tag{63}$$

$$\mathbf{0} = \frac{\mathrm{d}g}{\mathrm{d}\boldsymbol{E}} = \phi'\cdot\cdot\,\frac{\partial\boldsymbol{E}_{\mathrm{crit}}}{\partial\boldsymbol{E}}, \tag{64}$$

with $\mathbb{I}^S$ being the fourth-order identity on symmetric second-order tensors. The system of 36+6 linear equations has 36+6 unknowns $\partial\boldsymbol{E}_{\mathrm{crit}}/\partial\boldsymbol{E}$ and $\partial\lambda/\partial\boldsymbol{E}$, while all other derivatives can be directly calculated. Rearranging Eq. (63) to

$$\frac{\partial\boldsymbol{E}_{\mathrm{crit}}}{\partial\boldsymbol{E}} = \mathbb{A}\cdot\cdot\left(\mathbb{I}^S - \phi'\otimes\frac{\partial\lambda}{\partial\boldsymbol{E}}\right), \qquad \mathbb{A} = (\mathbb{I}^S + \lambda\phi'')^{-1} \tag{65}$$

and inserting into Eq. (64) yields

$$\frac{\partial\lambda}{\partial\boldsymbol{E}} = \alpha^{-1}\phi'\cdot\cdot\,\mathbb{A}, \qquad \alpha = \phi'\cdot\cdot\,\mathbb{A}\cdot\cdot\,\phi' \tag{66}$$

which can be substituted in Eq. (65) to obtain

$$\frac{\partial\boldsymbol{E}_{\mathrm{crit}}}{\partial\boldsymbol{E}} = \mathbb{A} - \alpha^{-1}(\mathbb{A}\cdot\cdot\,\phi')\otimes(\mathbb{A}\cdot\cdot\,\phi'), \tag{67}$$

where possible simplifications by using the symmetries of $\boldsymbol{E}$ and $\mathbb{A}$ have been employed. One notes that $\partial\boldsymbol{E}_{\mathrm{crit}}/\partial\boldsymbol{E}$ has the projector property $\partial\boldsymbol{E}_{\mathrm{crit}}/\partial\boldsymbol{E}\cdot\cdot\,\phi' = \mathbf{0}$. This has been expected due to the fact that different $\boldsymbol{E}$ can be projected to the same $\boldsymbol{E}_{\mathrm{crit}}$.

2.4 Viscous regularization

Until now, the modeling is purely elastic. The augmentation with a kinetic relation is discussed now. Several regularizations are possible, each has its drawbacks and benefits. The viscous regularization has been proved to be a convenient modeling tool in many situations. In crystal plasticity (Hutchinson [32], Asaro [5], Böhlke [12]), it does not only regularize away the

Taylor problem of selecting a unique combination of slip systems which produce the plastic deformation, but instabilities due to softening resulting from the rotation of the crystal (geometric softening can easily cancel out strain hardening) are avoided as well. Further, by choosing a proper dependence on the strain rate, it can be regarded as a penalty method in perfect plasticity (Simo [53]), transforming the system of algebraic and differential equations into ordinary differential equations. The latter can be treated efficiently by established time integration algorithms. Here, the elastic law is extended by a viscous contribution by adding a strain rate sensitivity to the stresses. In the spatial description,

$$\boldsymbol{\sigma}_{\mathrm{v}} = \boldsymbol{f}(\boldsymbol{D}) \tag{68}$$

serves as starting point, with $\boldsymbol{D}$ being the symmetric part of the velocity gradient $\boldsymbol{L} = \dot{\boldsymbol{F}}\boldsymbol{F}^{-1}$. By assuming viscous isotropy, the viscous stresses can be decomposed into a volumetric and a distortional part

$$\boldsymbol{\sigma}_{\mathrm{v}} = \eta_1(\boldsymbol{D})\boldsymbol{D}^{\circ} + \eta_2(\boldsymbol{D})\boldsymbol{D}'. \tag{69}$$

There are several reasons to drop the first term. Firstly, in crystal elasticity and plasticity volume changes are very small. Secondly, a viscosity is physically induced by friction forces between particles that pass by each other, which does not happen in purely dilatational deformations of crystals. Moreover, the viscosity is added in order to regularize the material behavior when the material undergoes the simple shear deformation connected to the twin formation, which is isochoric. Therefore, the first term in Eq. (69) and, thus, the index of η_2 are not needed. Further, a Newtonian viscous relation is assumed,

$$\boldsymbol{\sigma}_{\mathrm{v}} = \eta\boldsymbol{D}'. \tag{70}$$

This is translated to the material description by using

$$\boldsymbol{\sigma}_{\mathrm{v}} = J^{-1}\boldsymbol{F}\boldsymbol{T}_{\mathrm{v}}\boldsymbol{F}^{T}, \quad J = \det(\boldsymbol{F}), \tag{71}$$

$$\boldsymbol{D} = \frac{1}{2}\boldsymbol{F}^{-T}\dot{\boldsymbol{C}}\boldsymbol{F}^{-1} \tag{72}$$

One obtains

$$\boldsymbol{T}_{\mathrm{v}} = \frac{J\eta}{2}\boldsymbol{F}^{-1}(\boldsymbol{F}^{-T}\dot{\boldsymbol{C}}\boldsymbol{F}^{-1})'\boldsymbol{F}^{-T} \tag{73}$$

$$= \frac{J\eta}{2}(\boldsymbol{F}^{-1}(\boldsymbol{F}^{-T}\dot{\boldsymbol{C}}\boldsymbol{F}^{-1} - \frac{1}{3}\mathrm{tr}(\boldsymbol{F}^{-T}\dot{\boldsymbol{C}}\boldsymbol{F}^{-1})\boldsymbol{I})\boldsymbol{F}^{-T}) \tag{74}$$

$$= \frac{J\eta}{2}(\boldsymbol{C}^{-1}\dot{\boldsymbol{C}}\boldsymbol{C}^{-1} - \frac{1}{3}\mathrm{tr}(\boldsymbol{C}^{-1}\dot{\boldsymbol{C}})\boldsymbol{C}^{-1}). \tag{75}$$

By using that $\boldsymbol{C} \approx \boldsymbol{I}$, one can simplify the latter to

$$\boldsymbol{T}_{\mathrm{v}} = \frac{J\eta}{2}(\dot{\boldsymbol{C}} - \frac{1}{3}\mathrm{tr}(\dot{\boldsymbol{C}})\boldsymbol{I}) \tag{76}$$

$$= \frac{J\eta}{2}\dot{\boldsymbol{C}}'. \tag{77}$$

Adding $\boldsymbol{T}_{\mathrm{v}}$ to the elastic law yields

$$\boldsymbol{T} = \frac{\partial\tilde{w}}{\partial\boldsymbol{E}} + \boldsymbol{T}_{\mathrm{v}}. \tag{78}$$

The mathematical treatment of pseudoelasticity combined with a viscous contribution is challenging, even in the one dimensional case (Ericksen's bar, [21]). The case of a strictly monotonic increasing elastic law combined with a linear viscosity has been considered by Greenberg [26–28], who showed the existence, uniqueness, and stability of global solutions. Dafermus [19] analyzed the dynamic one-dimensional viscoelastic bar in a more general way, and found that the viscous part dominates the elastic part and secures the existence of a unique solution in the large, and that this solution is asymptotically stable in the sense that as t tends to ∞ the stresses and time derivatives of the displacement vanish. Moreover, the positive viscosity ensures the compliance of the Clausius-Duhem-inequality. Further studies of Ericksen's viscoelastic bar have been undertaken by Andrews [3, 4], Pego [44], and Ball [10].

Energy conservation is a basic principle in physics. However, it is not necessary to model the temperature increase due to internal friction (e.g. by dislocation movement) if it is not of interest. The viscous regularization models the thermal dissipation in a relatively simple manner. Summarising roughly, the viscous regularization is physically reasonable and mathematically helpful. Alternatively, one could think of the dynamic regularization, i.e., to no more neglect inertial forces. Although physically sound, the latter is less common. This is due to the more complicated analytical and numerical treatment compared to the viscous regularization.

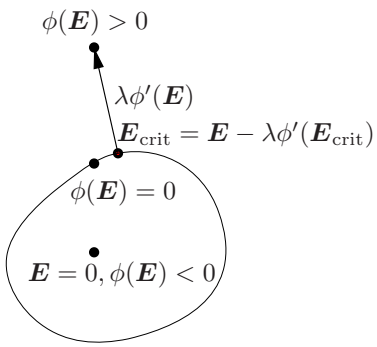

Fig. 6 Orthogonal projection to a critical strain state.

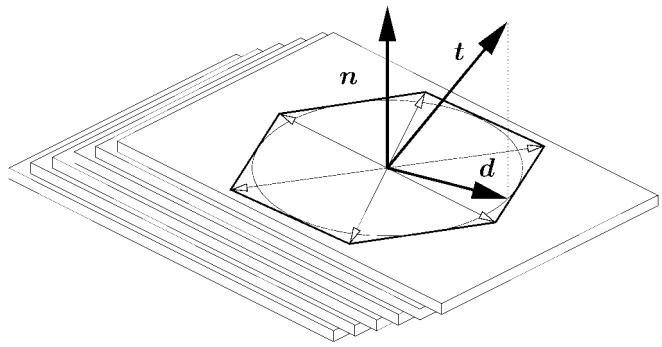

Fig. 7 Card glide mechanism.

2.5 Incorporation of crystallographic glide into the model

In magnesium, below 225°C slip occurs mainly along the $\langle\bar{2}110\rangle$, $\langle 1\bar{2}10\rangle$, and $\langle 11\bar{2}0\rangle$ directions in the basal $\{0001\}$ plane (Emley [20]). Due to the regular alignment of the slip systems in only one slip plane it is reasonable to approximate the collective of slip systems by the card glide mechanism, Fig. 7. It is assumed that slip occurs in the direction of the largest shear stress in the slip plane, like being observed on a card deck. Following Bertram [11] and Böhlke [13], the shear stress is given by

$$\tau = \tilde{\boldsymbol{F}}^T \boldsymbol{\sigma} \tilde{\boldsymbol{F}}^{-T} \cdot\cdot\, \boldsymbol{d} \otimes \boldsymbol{n}, \qquad \tilde{\boldsymbol{F}} = \boldsymbol{F}\boldsymbol{P}. \tag{79}$$

The direction $\boldsymbol{d}$ corresponding to the largest largest shear stress in the plane $\boldsymbol{n}$ is given by projecting the traction $\tilde{\boldsymbol{F}}^T \boldsymbol{\sigma} \tilde{\boldsymbol{F}}^{-T} \boldsymbol{n}$ into the $\boldsymbol{n}$-plane,

$$\boldsymbol{d} = (\boldsymbol{I} - \boldsymbol{n} \otimes \boldsymbol{n}) \tilde{\boldsymbol{F}}^T \boldsymbol{\sigma} \tilde{\boldsymbol{F}}^{-T} \boldsymbol{n}. \tag{80}$$

The evolution of the plastic transformation, which is a material variable (i.e. invariant with respect to Euclidean transformations), is given by

$$-\boldsymbol{P}^{-1}\dot{\boldsymbol{P}} = \dot{\gamma}\boldsymbol{d}^* \otimes \boldsymbol{n}, \qquad \boldsymbol{d}^* = \frac{\boldsymbol{d}}{\|\boldsymbol{d}\|}. \tag{81}$$

If $\boldsymbol{d}^*$ and $\boldsymbol{n}$ are constant, one obtains with $\boldsymbol{P}(t=0) = \boldsymbol{P}_0$ a solution for $\boldsymbol{P}$, namely

$$\boldsymbol{P} = \boldsymbol{P}_0(\boldsymbol{I} - \gamma\boldsymbol{d}^* \otimes \boldsymbol{n}), \tag{82}$$

This leaves only $\gamma(t)$ to be determined consistent with the elastic or viscoelastic law. In terms of resolved shear stresses, one has to employ $\tau_{\mathrm{el}} = \tau_{\mathrm{basal}}$. In the case of perfect plasticity, τ_{basal} is a function of γ, or, without hardening, τ_{basal} is constant. In the viscoelastic case, τ_{basal} depends on γ and $\dot{\gamma}$, or only on $\dot{\gamma}$ if hardening is ignored. In this work a perfect plastic behavior is preferred, since it can be resolved more easily in this quasi 1D-case. Due to the fact that the twin lamellae are mostly thin and dislocation free, basal slip is assumed to be potentially active only in the parent configuration (see, e.g., Shiekhelsouk [49]).

2.6 Final constitutive equations

In this section, the model derived in the last sections is summarized. The index 0 indicates the parent configuration, while the indices $1...n$ run over the possible twin variants. The simplifications $\boldsymbol{C} = \boldsymbol{I}$ and $\tilde{\boldsymbol{C}} = \boldsymbol{I}$ are employed. All sums are explicitly written. The strain energy density is given by

$$\tilde{w} = \sum_{i=0}^{n} a_i w_i \qquad a_i = \frac{g_i}{\sum_{j=0}^{n} g_j} \qquad g_i = \frac{h(w_i)}{1 - h(w_i)} \qquad h_i = \exp(-k w_i), \tag{83}$$

with k being a preferably large regularization parameter. The w_i are given by

$$w_i = \frac{1}{2}\boldsymbol{E}_i \cdot\cdot\, \mathbb{C}_0 \cdot\cdot\, \boldsymbol{E}_i \qquad \text{if } \phi_i(\boldsymbol{E}_i) \leq 0, \tag{84}$$

$$w_i = \boldsymbol{E}_i \cdot\cdot\, \mathbb{C}_0 \cdot\cdot\, \boldsymbol{E}_{i,\mathrm{crit}} - \frac{1}{2}\boldsymbol{E}_{i,\mathrm{crit}} \cdot\cdot\, \mathbb{C}_0 \cdot\cdot\, \boldsymbol{E}_{i,\mathrm{crit}} \qquad \text{if } \phi_i(\boldsymbol{E}_i) > 0, \tag{85}$$

according to the phenomenological model adaption of the strain energies. $\mathbb{C}_0$ is the elasticity tetrad. $\boldsymbol{E}_{\mathrm{crit}i}$ are given implicitly by the projection

$$\boldsymbol{E}_{i,\mathrm{crit}} = \boldsymbol{E}_i - \lambda\phi_i'(\boldsymbol{E}_{i,\mathrm{crit}}), \qquad \phi_i(\boldsymbol{E}_{i,\mathrm{crit}}) = 0, \tag{86}$$

where λ needs to be calculated such that the latter equations hold. The functions ϕ_i are

$$\phi_0(\boldsymbol{E}_0) = \sum_{j=1}^{n} \langle \gamma_j/\gamma_{\mathrm{twin}}\rangle^m - 1 \qquad \gamma_j = 2\boldsymbol{E}_0 \cdot\cdot\, \boldsymbol{M}_j, \tag{87}$$

$$\phi_i(\boldsymbol{E}_i) = \gamma_i - \gamma_{\mathrm{twin}} \qquad \gamma_i = 2\boldsymbol{E}_i \cdot\cdot\, \boldsymbol{M}_i \qquad i = 1...n, \tag{88}$$

with the preferably large regularization parameter m and a critical shear strain γ_{twin}. Green's strains $\boldsymbol{E}_i$ are obtained by

$$\boldsymbol{E}_i = \frac{1}{2}(\boldsymbol{P}_i^T \boldsymbol{C} \boldsymbol{P}_i - \boldsymbol{I}). \tag{89}$$

The elastic isomorphisms map the elastic reference law to the reference placement. $\boldsymbol{P}_0$ is given by the parent crystal orientation, and $\boldsymbol{P}_i,\ i = 1...n$ are given by

$$\boldsymbol{P}_i = \boldsymbol{P}_0 \boldsymbol{P}_{0i} \qquad i = 1...n, \tag{90}$$

with the plastic transformations $\boldsymbol{P}_{0i}$

$$\boldsymbol{P}_{0i} = -\boldsymbol{I} - \gamma_0 \boldsymbol{d}_i \otimes \boldsymbol{n}_i + 2\boldsymbol{n}_i \otimes \boldsymbol{n}_i \qquad i = 1...n, \tag{91}$$

which map the elastic reference law to the twin configurations, see Eq. (49) and Fig. 5. With $\tilde{w}$ on hand by the latter system of equations, the second Piola Kirchhoff stresses are

$$\boldsymbol{T} = \frac{\partial \tilde{w}}{\partial \boldsymbol{E}} \approx \sum_{i=0}^{n} a_i \boldsymbol{T}_i, \tag{92}$$

$$\boldsymbol{T}_i = \frac{\partial w_i}{\partial \boldsymbol{E}} = \boldsymbol{P}_i \frac{\partial w_i}{\partial \boldsymbol{E}_i} \boldsymbol{P}_i^T. \tag{93}$$

This is, so far, the elastic law. Incorporating the viscous regularization corresponds to adding the deviatoric part of $\frac{J\eta}{2}\dot{\boldsymbol{C}}$ to the second Piola Kirchhoff stresses. Regarding the card glide mechanism, the plastic transformation of the parent evolves corresponding to

$$-\boldsymbol{P}_0^{-1}\dot{\boldsymbol{P}}_0 = \dot{\gamma}\boldsymbol{d}^* \otimes \boldsymbol{n}, \qquad \boldsymbol{d}^* = \frac{\boldsymbol{d}}{\|\boldsymbol{d}\|}, \tag{94}$$

with

$$\boldsymbol{d} = ((\boldsymbol{I} - \boldsymbol{n} \otimes \boldsymbol{n})\tilde{\boldsymbol{F}}^{-1}\boldsymbol{\sigma}\tilde{\boldsymbol{F}}^{-T}) \cdot \boldsymbol{n}, \qquad \tilde{\boldsymbol{F}} = \boldsymbol{F}\boldsymbol{P}_0. \tag{95}$$

$\dot{\gamma}$ is determined consistently with the elastic law. I.e., during the plastic flow, the resolved shear stress in the card glide system is equal to the flow stress.

Numerical treatment of the card glide mechanism. In the remainder of this paragraph the numerical treatment of the card glide mechanism is sketched. $\boldsymbol{d}$ is given by Eq. (95), with $\boldsymbol{n}$ being the normalized $\boldsymbol{c}$ direction of the hexagonal unit cell. The resolved shear stress, the yield condition and the loading condition are

$$\tau_{\mathrm{el}} = \sqrt{\boldsymbol{d} \cdot \boldsymbol{d}}, \qquad 0 = \tau_{\mathrm{el}} - \tau_{\mathrm{basal}} = \phi(\tau_{\mathrm{el}}, \tau_{\mathrm{basal}}), \qquad \dot{\phi} > 0. \tag{96}$$

If both conditions are fulfilled, $\boldsymbol{P}_0$ evolves. Otherwise the deformation is viscoelastic, and $\dot{\boldsymbol{P}}_0 = \boldsymbol{0}$. While $\boldsymbol{P}_0$ evolves, the consistency condition $\dot{\phi} = 0$ must hold. When elastoplasticity is treated numerically, one does not obtain a continuous evolution of $\boldsymbol{P}_0$ but a sequence of discrete $\boldsymbol{P}_0^n$. Therefore the consistency condition and the loading condition enter the

numerical considerations in the following manner. Being given a strain increment $\boldsymbol{P}_0^n, \boldsymbol{F}^n$, and $\boldsymbol{F}^{n+1}$, a predictor step is carried out, where $\boldsymbol{P}_0^{n+1} = \boldsymbol{P}_0^n$ is assumed. In this way, one treats the strain increment as fully viscoelastic, and calculates the resolved shear stress τ_{el}^{n+1} as given above. Then, if

$$\tau_{\mathrm{el}}^{n+1} > \tau_{\mathrm{basal}}^n \tag{97}$$

is fulfilled, $\boldsymbol{P}_0^{n+1}$ has to be determined such that $\tau_{\mathrm{el}}^{n+1} = \tau_{\mathrm{basal}}^{n+1}$ and $\det(\boldsymbol{P}_0^{n+1}) = 1$. Here, only one slip system is considered, i.e., one can make use of Eq. (82), and write

$$\boldsymbol{P}_0^{n+1} = \boldsymbol{P}_0^n(\boldsymbol{I} - \Delta\gamma \boldsymbol{d}^* \otimes \boldsymbol{n}), \tag{98}$$

where $\boldsymbol{d}^*$ is the normalized $\boldsymbol{d}$ from the predictor step. In order to respect isotropic hardening, it is assumed that τ_{basal} depends on the accumulated shear

$$\gamma_{\mathrm{acc},n+1} = \gamma_{\mathrm{acc},n} + |\Delta\gamma|, \tag{99}$$

which is an internal variable. One can determine the scalar variable $\Delta\gamma$ such that the scalar equation $\tau_{\mathrm{el}}^{n+1} = \tau_{\mathrm{basal}}^{n+1}$ holds by Newtons method, or, slower convergent but more stable, by the bisection method. The fact that only one scalar equation has to be solved renders the card glide mechanism in this case as fairly fast and stable. As mentioned before, basal glide is taken into account only in the parent configuration, i.e., it remains to discuss how this can be implemented. For this purpose, the indicator function ϕ_n from the elastic law is used. ϕ_n is equal to -1 in the stress free parent configuration, and grows with the regularization exponent m, as the strain state diverges from this state. It is 0 when the critical strain state is reached. By defining $\tau_{\mathrm{basal}} = (\phi + 2)\tau_{\mathrm{basal0}}$, one obtains a virtually unreachable resolved shear stress when the critical strain is passed, while leaving τ_{basal} approximately unaltered in subcritical strain region. Although this treatment appears empirical at the first glance, it can be interpreted as a regularization of the algebraic condition that slip is only possible in the parent configuration, i.e., as long as $\phi_0(\boldsymbol{E}_0) < 0$. When the regularization parameter $m \to \infty$ in ϕ_n (Eq. (56)), $\tau_{\mathrm{basal}} = \tau_{\mathrm{basal0}}$ due to $\phi_0 \to -1$ for subcritical strain states, and $\tau_{\mathrm{basal}} \to \infty$ if a critical strain state is passed. Algebraic formulations are, however, not preferable from a numerical point of view, which is why the latter regularized formulation is used in this work.

In order not to overload the model by too many ingredients, hardening has been generally neglected, i.e. $\tau_{\mathrm{basal0}} =$ constant. In the remainder, τ_{basal0} is a material parameter, and the index 0 is omitted.

2.7 Material parameters

The material parameters are given with respect to the elastic reference law. $\boldsymbol{e}_1$ is parallel to $\boldsymbol{a}_1$ while $\boldsymbol{e}_3$ is parallel to the $\boldsymbol{c}$-axis. The elastic stiffness tetrad of magnesium (Simmons [52]), with respect to the basis $\boldsymbol{B}_1 = \boldsymbol{e}_1 \otimes \boldsymbol{e}_1$, $\boldsymbol{B}_2 = \boldsymbol{e}_2 \otimes \boldsymbol{e}_2$, $\boldsymbol{B}_3 = \boldsymbol{e}_3 \otimes \boldsymbol{e}_3$, $\boldsymbol{B}_4 = \sqrt{2}/2(\boldsymbol{e}_1 \otimes \boldsymbol{e}_2 + \boldsymbol{e}_2 \otimes \boldsymbol{e}_1)$, $\boldsymbol{B}_5 = \sqrt{2}/2(\boldsymbol{e}_1 \otimes \boldsymbol{e}_3 + \boldsymbol{e}_3 \otimes \boldsymbol{e}_1)$, $\boldsymbol{B}_6 = \sqrt{2}/2(\boldsymbol{e}_2 \otimes \boldsymbol{e}_3 + \boldsymbol{e}_3 \otimes \boldsymbol{e}_2)$ is

$$\mathbb{C} = \begin{bmatrix} 56.49 & 23.16 & 18.10 & 0 & 0 & 0 \\ & 56.49 & 18.10 & 0 & 0 & 0 \\ & & 58.73 & 0 & 0 & 0 \\ & & & 2 \times 16.81 & 0 & 0 \\ & & & & 2 \times 16.81 & 0 \\ & & & & & 56.49 - 23.16 \end{bmatrix} \boldsymbol{B}_i \otimes \boldsymbol{B}_j, \tag{100}$$

in GPa. $\boldsymbol{B}_i$ is an orthonormal vector basis for symmetric second-order tensors, i.e. a fourth-order tensor with both sub-symmetries can be denoted as a second-order tensor with respect to $\boldsymbol{B}_i$. The six structural tensors belonging to the $\{10\bar{1}2\}\langle\bar{1}011\rangle$ twin systems are given by

$$\boldsymbol{M}_1 = \boldsymbol{d}_1 \otimes \boldsymbol{n}_1, \tag{101}$$

$$\boldsymbol{d}_1 = \cos(\alpha)\boldsymbol{e}_2 + \sin(\alpha)\boldsymbol{e}_3, \tag{102}$$

$$\boldsymbol{n}_1 = -\sin(\alpha)\boldsymbol{e}_2 + \cos(\alpha)\boldsymbol{e}_3, \tag{103}$$

$$\boldsymbol{M}_i = \boldsymbol{Q}_{\pi/3\boldsymbol{e}_3}^{i-1} * \boldsymbol{M}_1, \qquad i = 2...6, \tag{104}$$

i.e. by rotating the twin system $\boldsymbol{M}_1$ in the sixfold symmetric hexagonal cell, with

$$\alpha = \arctan(c/(a\sqrt{3})). \tag{105}$$

For magnesium and its alloys, $c/a \approx 1.623$. The twinning shear for the $\{10\bar{1}2\}\langle\bar{1}011\rangle$ twin systems is given by

$$\gamma_0 = \frac{\sqrt{3}}{c/a} - \frac{c/a}{\sqrt{3}}, \tag{106}$$

i.e. $\gamma_0 \approx 0.13$. The regularization parameter k and the viscosity are taken as $k = 0.025$ and $\eta = 10000$ MPa s, if nothing else is stated.

The regularization parameter of the phenomenological model adaption of the strain energy (as discussed in Sect. 2.3) is taken to be $m = 10$. The used critical shear strain is $\gamma_{\text{twin}} = 0.05\gamma_0$. The critical shear stress for twinning is therefore approximately $\tau_{\text{crit}} = G\gamma_{\text{twin}} \approx 0.05 \times 0.13 \times 17000$ MPa ≈ 110 MPa.

For the basal glide, only the critical shear stress τ_{basal} enters the card glide. It is observed that the critical $\{10\bar{1}2\}\langle\bar{1}011\rangle$ twinning stress and the basal slip shear stress are related by $\tau_{\text{crit}}/\tau_{\text{basal0}} \approx 4$. Therefore, τ_{basal} is set to 30 MPa.

2.8 Elastic energy invariance

The elastic modeling of twinning has been firstly tackled by Ericksen [21–23] and Zanzotto [58,59]. With the argument that parent and twin consist of the same material, Zanzotto refers to the $\boldsymbol{P}_i$ (what we consider here as elastic isomorphism) as material symmetry operations. For many materials he found that these invade, together with the symmetry operations of the lattice, the whole unimodular group, which is the material symmetry group of elastic fluids. In other words, any isochoric deformation can be achieved to be stress free by a series of twinning operations. Therefore, it is clear that one has to restrict the allowed twinning operations somehow. In this work, we incorporate only first-order twins, which relieves the situation mostly. Still, a shifting from one twin configuration to another one without passing by the parent configuration may occur, which is demonstrated later on. Moreover, even if one is restricted to first-order twins, one has to deal with an elastic energy invariance. In the usual twin notation (Pitteri [46]), the shearing occurs along plane $\boldsymbol{k}_1$, while the second undistorted plane $\boldsymbol{k}_2$ is flipped over to $\boldsymbol{k}_2'$. If one interchanges the planes, i.e. shearing along plane $\boldsymbol{k}_2$ and turning over $\boldsymbol{k}_1$, one obtains the conjugate twinning mode.

For conjugate twins with the isomorphisms $\boldsymbol{P}$ and $\boldsymbol{P}^*$ one can show that the elastic energies $w = w_0(\boldsymbol{P}^T * \boldsymbol{C})$ and $w^* = w_0(\boldsymbol{P}^{*T} * \boldsymbol{C})$ differ by a two fold rotation $\boldsymbol{R}_{(\boldsymbol{d}\times\boldsymbol{n})}$ of $\boldsymbol{C}$ inside the common plane of shear. Because of $\boldsymbol{R}_{(\boldsymbol{d}\times\boldsymbol{n})} = \boldsymbol{R}_{\boldsymbol{n}}\boldsymbol{R}_{\boldsymbol{d}}$, this rotation must be an element of the lattice symmetry group if the twinning modes are compound twins (Stark [54]). This leads to the conclusion that conjugate compound twins are not distinguishable in terms of the elastic energy.

One has to pay special attention on the effect of the latter energy invariance. If, in the usual twin notation, the planes $\boldsymbol{k}_1, \boldsymbol{k}_2$ and directions $\boldsymbol{\eta}_1, \boldsymbol{\eta}_2$ are crystallographically equivalent, the elastic energy invariance couples crystallographically equivalent twinning modes. This is the case for many twinning modes in highly symmetric lattices (bcc, fcc, hcp). The six $\{01\bar{1}2\}\langle 0\bar{1}11\rangle$ twin systems considered in this work are formed by three pairs of crystallographically equivalent conjugate twin systems. Although, by means of elasticity, the conjugate twins cannot be distinguished at the level of a material point, one can identify the twins by looking at the interface alignment, which is demonstrated later on.

If $\boldsymbol{k}_1, \boldsymbol{k}_2$ and $\boldsymbol{\eta}_1, \boldsymbol{\eta}_2$ are crystallographically distinct, the elastic energy invariance connects crystallographically distinct twinning modes. For example, the six commonly observed $\{01\bar{1}1\}\langle 01\bar{1}\bar{2}\rangle$ twin systems (compression twins in Mg) are opposed by the six $\{01\bar{1}\bar{3}\}\langle 03\bar{3}2\rangle$ twin systems. Both twinning modes show different characteristics, but are connected by the elastic energy invariance. Therefore, by incorporating the $\{01\bar{1}1\}\langle 01\bar{1}\bar{2}\rangle$ twin systems into $\tilde{w}$, one automatically enables $\{01\bar{1}\bar{3}\}\langle 03\bar{3}2\rangle$ twinning to identical conditions. Therefore, it appears reasonable to apply the elastic modeling only to non-compound twin systems and compound twin systems which are formed by crystallographically equivalent twin systems.

3 Numerical examples

3.1 Simple shear tests in a twin system and the basal plane

Before any structural problem is solved with the FEM, it should be investigated how the material model behaves in an entirely strain-driven test, and how stresses and internal variables evolve if $\boldsymbol{F}(t)$ is prescribed. Most interesting is a shear test in one of the six twin systems. Therefore,

$$\boldsymbol{F} = \boldsymbol{I} + \gamma \boldsymbol{d}_1 \otimes \boldsymbol{n}_1, \qquad \boldsymbol{P}_0 = \boldsymbol{I} \tag{107}$$

is imposed, with $0 < \gamma < \gamma_0$. $\boldsymbol{P}_0 = \boldsymbol{I}$ indicates that the elastic law in the reference configuration is identical to the current elastic reference law. Since we do not solve the pseudoelastic boundary value problem, but carry out a strain driven test,

the problem is not ill posed, which permits to omit the viscosity. This enables us to verify the adaption of the material parameters of the elastic law. For the same reason, basal glide is deactivated as well. In Fig. 8 the shear stress in the twin system $\tau_1 = \boldsymbol{\sigma} \cdot\cdot (\boldsymbol{d}_1 \otimes \boldsymbol{n}_1)$ is plotted over γ, with the Cauchy stresses $\boldsymbol{\sigma}$. The regularization parameter k, which smoothens the transitions between the different elastic laws, has been varied.

One recognizes that the material is stress-free when the twin configuration is reached, and that the elastic behavior is linear near the stress-free states. The parameter k influences the sharpness of the transition between the elastic laws, as it is expected from the regularization. As the transition phase, which is smoothed by the regularization parameter k, corresponds to the nonconvex region (with a negative stiffness) no stable equilibrium configuration can be found in that interval. It merely serves as the transition zone. It is therefore reasonable to choose k large enough such that the elastic laws near the stress free configurations are represented sufficiently well, but small enough to have a smooth transition between the twin and parent configuration. Therefore, for the simulations that are presented in the following sections, $k = 0.025$ has been chosen.

It is further important to review the effect of the phenomenological model adaption. Therefore, it has been incorporated with the critical critical shear strain is $\gamma_{\text{twin}} = 0.05\gamma_0$. The critical shear stress results to fit well the prior estimation of approximately 110 MPa, see Fig. 8. One notes that the phenomenological model adaption limits the stresses.

In order to review the basal glide, a cyclic test with

$$\boldsymbol{F} = \boldsymbol{I} + \gamma \boldsymbol{a}_1 \otimes \boldsymbol{c}^*, \qquad \boldsymbol{P} = \boldsymbol{I} \tag{108}$$

has been carried out, with γ evolving linearly from 0 to 0.025 and back to 0. As the reference placement and the elastic reference law coincide again, $\boldsymbol{a}_1 = \boldsymbol{e}_1$ and $\boldsymbol{c}^* = \boldsymbol{e}_3$ are chosen. The resolved shear stress plotted in Fig. 8 corresponds therefore to the component σ_{13} when $\boldsymbol{\sigma}$ is given with respect to the basis $\boldsymbol{e}_i$. One clearly recognizes the ideal plastic behavior as the card glide mechanism is activated, with $\tau_{\text{crit}} = 30$ MPa.

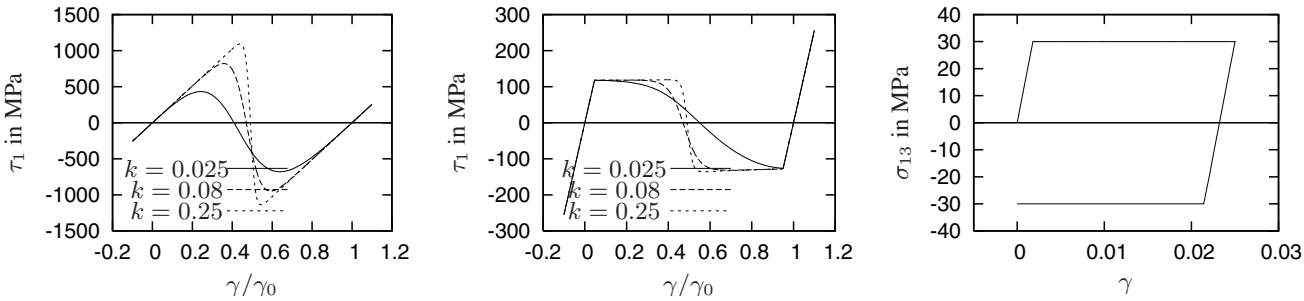

Fig. 8 Resolved shear stress in MPa in twin system one over γ, without (left) and with (center) the phenomenological model adaption, resolved shear stress in a shear test within the basal plane, with $\tau_{\text{crit}} = 30$ MPa (right).

3.2 Implementation into a finite element system

To solve the quasistatic pseudoelastic boundary value problem, the material law has been implemented as a "user material subroutine" in the FE-System ABAQUS/STANDARD. Different element types have been used, which are given in the model setup of each FE model. The derivative

$$\mathbb{C}_{ABQ} = \frac{1}{J} \frac{\partial \boldsymbol{\tau}_{n+1}}{\partial \Delta \boldsymbol{\varepsilon}} \tag{109}$$

required by ABAQUS, with the Kirchhoff stresses $\boldsymbol{\tau}$ and the spacial logarithmic strains $\boldsymbol{\varepsilon}$, has been approximated by

$$\mathbb{C}_{ABQ} \approx \frac{1}{J} \frac{\partial \boldsymbol{F}_{n+1} \boldsymbol{T}_{n+1} \boldsymbol{F}_{n+1}^T}{\partial \boldsymbol{C}_{n+1}} |_{\Delta t = \text{const}} \cdot\cdot \frac{\partial \boldsymbol{C}_{n+1}}{\partial \Delta t \boldsymbol{D}} \tag{110}$$

$$= \frac{1}{J} \frac{\partial \boldsymbol{F}_{n+1} \boldsymbol{T}_{n+1} \boldsymbol{F}_{n+1}^T}{\partial \boldsymbol{C}_{n+1}} |_{\Delta t = \text{const}} \cdot\cdot \frac{\partial \dot{\boldsymbol{C}}}{\partial \boldsymbol{D}} \tag{111}$$

$$= \frac{1}{J} \frac{\partial \boldsymbol{F}_{n+1} \boldsymbol{T}_{n+1} \boldsymbol{F}_{n+1}^T}{\partial \boldsymbol{C}_{n+1}} |_{\Delta t = \text{const}} \cdot\cdot \frac{\partial 2 \boldsymbol{F}^T \boldsymbol{D} \boldsymbol{F}}{\partial \boldsymbol{D}} \tag{112}$$

$$\approx \frac{2}{J} \boldsymbol{F} * \frac{\partial \boldsymbol{T}_{n+1}}{\partial \boldsymbol{C}_{n+1}} |_{\Delta t = \text{const}} \cdot \tag{113}$$

From Eq. (112) to (113), two of the three derivatives from the remaining product have been neglected, since they are of much lower order (stresses) compared to the remaining one (stiffness). The latter representation of $\mathbb{C}_{ABQ}$ is advantageous if the material law is formulated in terms of material quantities.

3.3 FE Model 1: Simple shear deformation into one twin system

3.3.1 Model setup

In this section, the fully deformation-controlled simple shear test from the last section is extended to a structural problem. A strip of the dimensions 100 mm×200 mm×3 mm is submitted to a simple shear deformation, see Fig. 9. The boundary conditions are such that a plane strain deformation is enforced, so that the problem is two-dimensional. Therefore along the thickness direction only one element has been assigned. The lattice is oriented such that the shear plane coincides with one of the six equivalent $\{10\bar{1}2\}$ twinning planes and that twinning can occur in the direction of the enforced shear direction. The displacement boundary conditions are such that one face is fixed, while the opposing face is displaced parallel and proportional to time by finally 15 mm in 1000 seconds, and back to zero in 1000 seconds. A small notch at one of the free boundaries serves as a perturbation to trigger the twin formation. Different meshes have been been used, namely a regular hexahedral mesh with linear shape functions (element type C3D8) and irregular wedge meshes with linear and quadratic shape functions (element types C3D6 and C3D15).

The maximal displacement due to the twinning shear deformation is $\gamma_0 \times 100$ mm. With $\gamma_0 \approx 0.13$, the faces should be displaced at least 13 mm in order to enforce the entire twinning of the sample. The simulations are carried out with different meshes, varying the characteristic element size, the degree of the shape functions in the elements, and the viscosity in the material law.

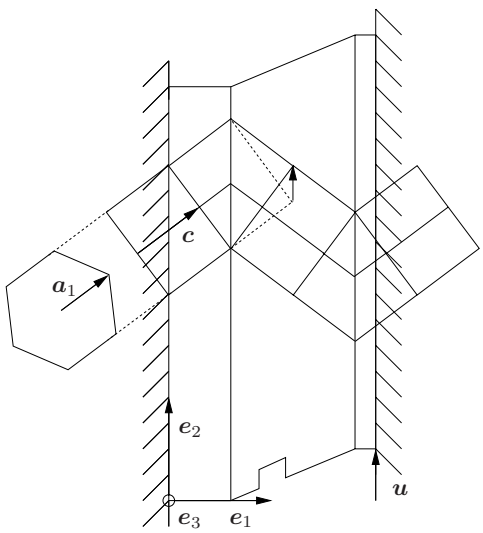

Fig. 9 Simple shear deformation of a strip, with an oversized hexagonal cell. The lattice is oriented such that the shear plane coincides with one of the $\{10\bar{1}2\}$ twinning planes. A small notch is incorporated as preferred nucleation site.

3.3.2 Results

In the simulations a twin nucleates near the notch, and propagates along the shear direction. After invading the overall length of 200 mm, the twin starts growing in direction of the shear plane normal, i.e., the thickness of the twin grows, see Fig. 11. As the deformation is reversed, a similar detwinning-behavior is observed. It is pointed out that such ideal twinning and detwinning behavior is not observed in reality. The simulation should merely demonstrate the possibility of detwinning, the effect of the phenomenological model adaption, and the hysteresis.

The regularizing viscosity is so small in the context of this simulation that a variation of it has no significant influence. Its effect on the nominal stress can be estimated by $\tau_{\text{visc}} \approx \dot{\gamma}\eta/2 = 1.5\text{E} - 4\text{s}^{-1}\eta/2 = 0.3$ MPa. One notes that the nominal critical twinning shear stress of approximately 110 MPa suites to the value that was adjusted in Sect. 2.7.

Consider the nominal shear stress-displacement diagram 10. One notes that at the displacement of approximately 13 mm the entire specimen has been invaded by the twin, and that at ongoing deformation the elastic law of the twin is found. The distinct load drops in both diagrams are connected to the fineness of the mesh. Each load drop corresponds to the transition of the twin boundary from one element row to the next when the twin grows in thickness direction. Consequently, the coarser the mesh is, the larger is the load drop. Moreover, the twin parent interfaces are approximately parallel to mesh

interfaces, due to the mesh structure. This has an impact on the simulation results. In order to review the mesh-dependence in more detail, the simulations have been repeated with an irregular wedge mesh of moderate fineness, with linear and quadratic shape functions. The nominal shear stress over the displacement is depicted in Fig. 10, two particular interesting states are depicted in Fig. 12. Figure 10 shows the hysteresis connected to twinning and detwinning for an irregular mesh. At the onset of twinning and detwinning, the stress displacement curve fits quite well to the findings with the regular mesh. In the propagation stage, the first stress peak is not reached again, and the nominal shear stress stays below the approximately constant peak level that is found in the regular mesh simulations. This behavior is more realistic than the results with the regular meshing. The load drops are due to the mesh irregularity less pronounced.

The states depicted in Figs. 11 and 12 give a good impression on the mesh-dependence. It appears that in case of quadratic shape functions the mesh-dependence is less pronounced. The unrealistic thickening of the twin tips that are embedded according to the mesh interfaces are not encountered, neither the flipping of entire rows of elements.

While the overall behavior is as expected and mostly satisfactory, observed problems should not be concealed. In the following, "regular twin" means a twin which aligns its interface parallel to the shear direction, while a kink twin aligns its interface perpendicular to the shear direction. The kink twins are not observed in practice. In Fig. 11 one notes that in the first place an intermediate twin evolves perpendicular to the shear direction. As the model is elastic, this twin vanishes as the deformation continues, and is replaced by the regular twin. The intermediate twin appears only in the mesh of medium fineness. Further, due to the energy invariance of conjugate twins, it is not clear whether the intermediate twin should be regarded as a kink-twin variant of the twin that is aimed for, or as a regular twin of the twin system that is conjugate to the targeted twin. The conjugate twin systems have their shear planes aligned almost perpendicular to each other, namely at $86.3°$, while the mesh interfaces intersect at an angle of $90°$. Due to the mesh morphology it is reasonable to suppose that a regular twin propagates along a mesh interface if its shear plane is approximately parallel to it, i.e., the propagation direction depends on the meshing. It is therefore recommendable to use irregular meshes in conjunction with the present material model, in order to not induce a preferred twin-interface alignment. Moreover, the use of quadratic shape functions appears to ease the mesh-dependence as well. To review the mesh dependence in more detail, the nominal shear stress vs. displacement curve for three quadratic and irregular meshes of different fineness is depicted in Fig. 13. One sees that the unsteadiness is less pronounced at the finest mesh, where the amplitude of the load drops is lowest.

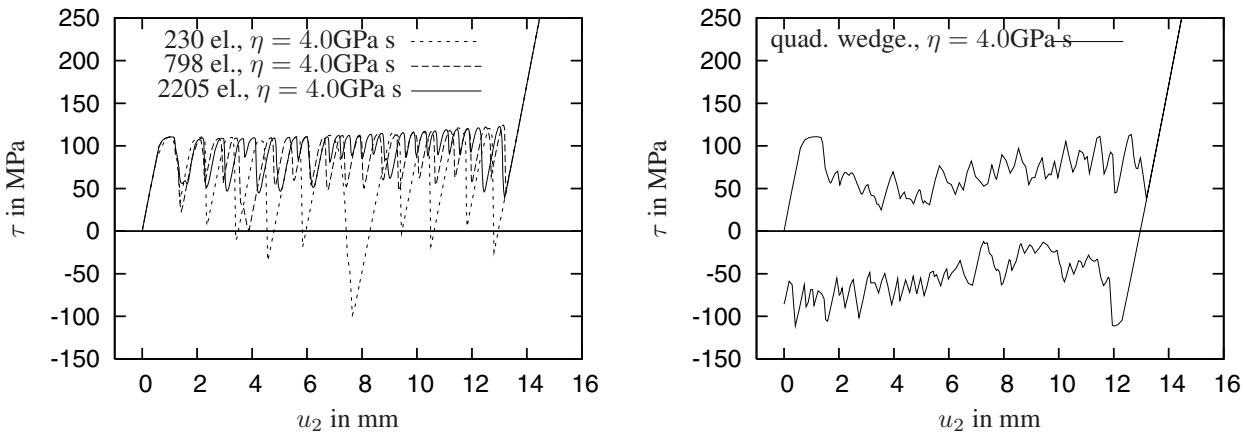

Fig. 10 Nominal shear stress vs. displacement for different regular hexahedral meshes with linear shape functions (left) and for the quadratic wedge mesh (right).

3.3.3 Unsteady twin formation

The existence of a peak stress at the twin nucleation, and a lower propagation stress level is in accordance with observations and theoretical considerations (Christian [17], Kochmann [35]). It is responsible for the burst-like propagation of newly formed twins. This behaviour is similar to the stick-slip phenomenon encountered in dry-friction, and has been verified experimentally (Boyko [15], Kawabata [33]) and by atomistic modelling (Hu [31]).

Even though no nucleation stress has been explicitly accounted for, the burst-like propagation is observed in the simulations. It is interesting to note that neither the nucleation nor the propagation stress depend on the fineness of the mesh, see Fig. 13. From the simulations it can be concluded that the load drop from the nucleation to the propagation level occurs as soon as the twin tips reach the free boundaries, and the twin propagation by advancing the two interfaces towards the parent

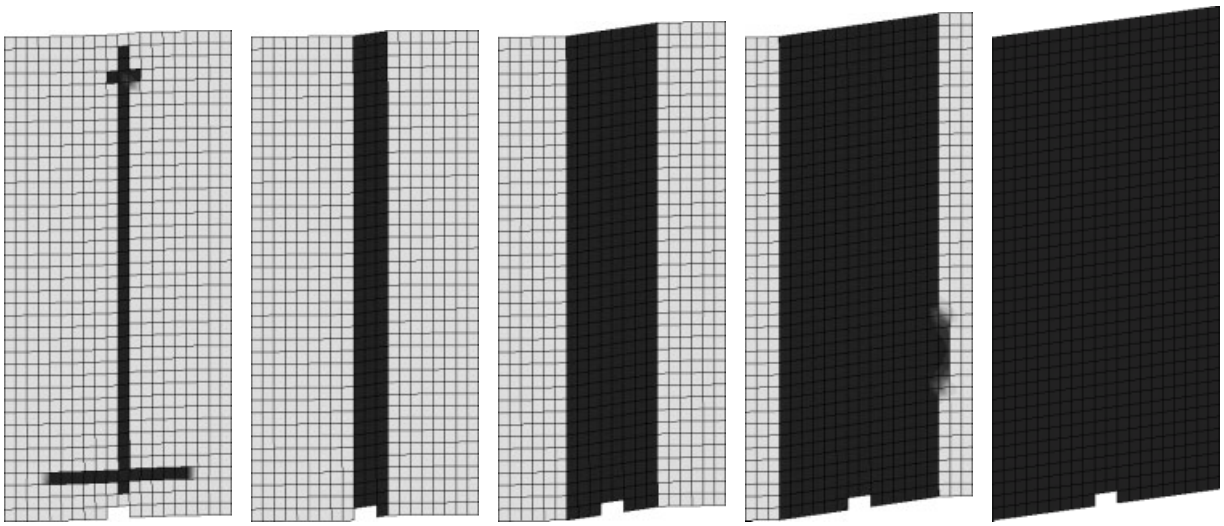

Fig. 11 Twin evolution from left to right at u =2.7 mm, 2.9 mm, 6.7 mm, 10.4 mm and 13 mm on the intermediate fine mesh. The grayscaling displays the weight factor corresponding to the parent configuration, (white) $0 < a_0 < 1$ (black). Note the intermediate twin at $u = 2.67$ mm, and the propagation of the interface into the next row recorded at $u = 10.4$ mm.

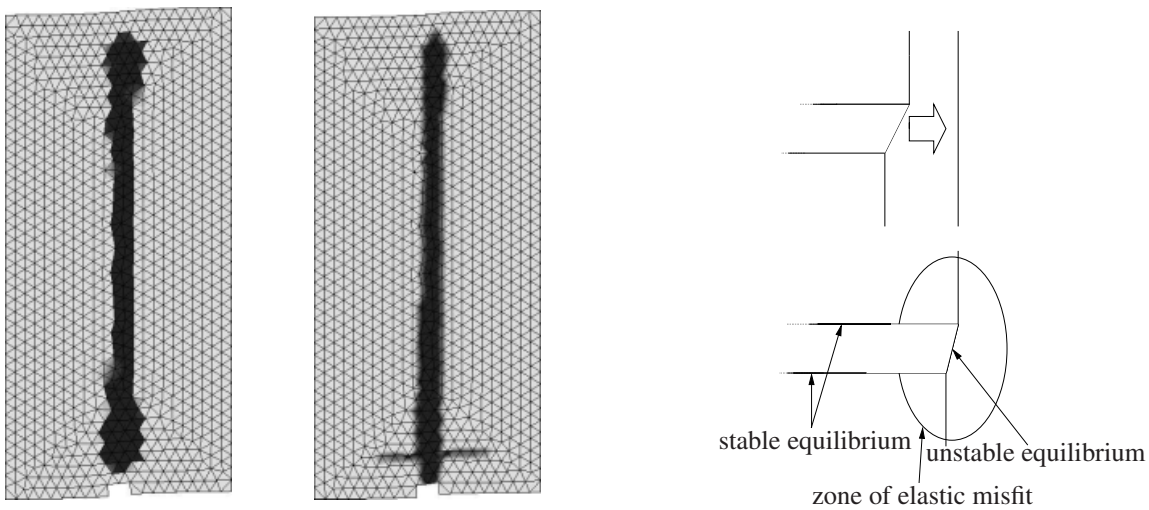

Fig. 12 Twin shortly after nucleation in the linear (left) and the quadratic (center) wedge mesh. Elastic misfit due to the twin nucleus (shaded, right).

phase starts. This behavior is quite realistic. E.g., if one looks at a micrograph of a twinned structure, one merely finds a free twin tip inside a grain.

The equilibrium at the interface between twin nucleus and parent is unstable (see Fig. 12 for a sketch). A small perturbation, like external loading or internal stresses, leads to interface motion. The fact that the twin tip shoots through the sample instead of advancing proportional with the application of the boundary conditions indicates that the elastic misfit strain caused by the twin triggers the twin propagation. The conclusion is that the elastic misfit can give the crucial stroke to the unstable equilibrium, which causes the observed shooting-through of the twin. In the simulations, the speed at which the twin tip shoots through is not infinite because of the viscous regularization. A reduction of the viscosity results in a shorter nucleation phase, respectively a faster shooting-through of the twin, see Fig. 13. In FE-simulations with a domino-row arrangement of elements, the twin propagation speed has been found to be inversely proportional to the viscosity.

Summarising roughly, the discrepancy between the nucleation- and propagation stress is partially caused by the elastic misfit strain around the twin nucleus, which pushes the neighboring parent phase towards the twin configuration. This results in a reduction of the stress that has to be applied to trigger the twin propagation, compared to the loading that is necessary to generate a twin nucleus from the uniform parent phase. The twin nucleation is controlled by the movement

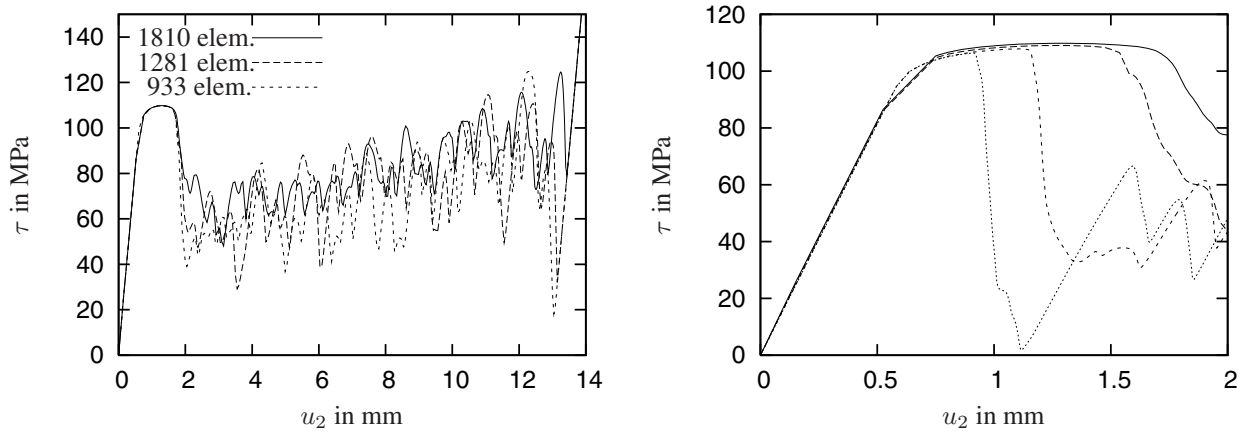

Fig. 13 Nominal shear stress vs. displacement for the quadratic wedge meshes of different fineness (left) and different viscosities ($\eta = \{1000$ MPa s, 2000 MPa s, 6000 MPa s, 10000 MPa s$\}$, right). The smaller the viscosity, the earlier occurs the load drop.

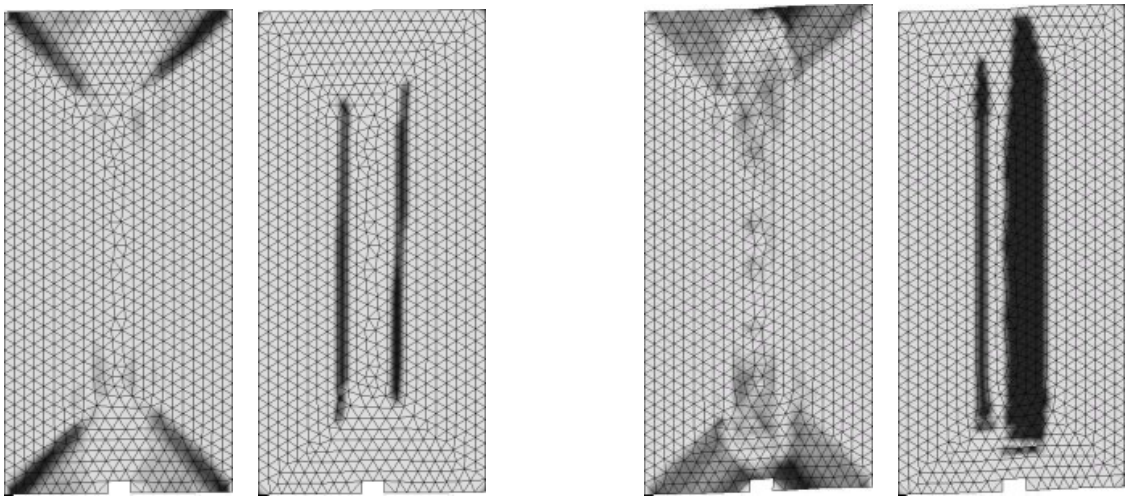

Fig. 14 Slip twin interaction at $t = 82.5$ s (left figures) and at $t = 224$ s (right figures). In each pair of figures, the left figure displays the accumulated basal shear (0...0.05 and 0...0.1) while the right figure displays the twin volume fraction (0...1).

and agglomeration of partial dislocations, which may occur at stresses that depart significantly from the propagation stress of an evolved twin.

3.3.4 Incorporation of basal glide

If basal glide is activated, the plane deforms initially by slip bands, which start at the corners and end inside the plane. Then, two twins develop such that they connect the ends of the slip bands, see Fig. 14. The shear bands deviate slightly from the orientation $\pm 45°$ with respect to the model edges, because the angle between the basal plane and the $\{10\bar{1}2\}$ plane (parallel to the displaced face) is $\approx 43.16°$.

3.4 FE Model 2: Elongation of a notched band

3.4.1 Model setup

The second FE model consists of a notched single crystal band, which is elongated along the length axis (Fig. 15). Again, a plane strain state is enforced by prescribing $u_1 = 0$ on the principal faces of the stripe, while the transverse displacement perpendicular to the thickness direction is not constrained. The notch is the inhomogeneity at which twins should nucleate. The hexagonal crystal lattice is aligned such that an edge of the base hexagon is parallel to the band normal, while the $\boldsymbol{c}$-axis deviates slightly from the length axis with the angle α. The non-zero displacement boundary condition is applied

proportional to time, which runs from 0 to 1000 s. Regular hexahedral meshings with linear and quadratic shape shape functions have been used (element types C3D8 and C3D20). The regular meshing is considered as not problematic, since the crystal orientation enforces an interface orientation which is far from parallel to the mesh interfaces.

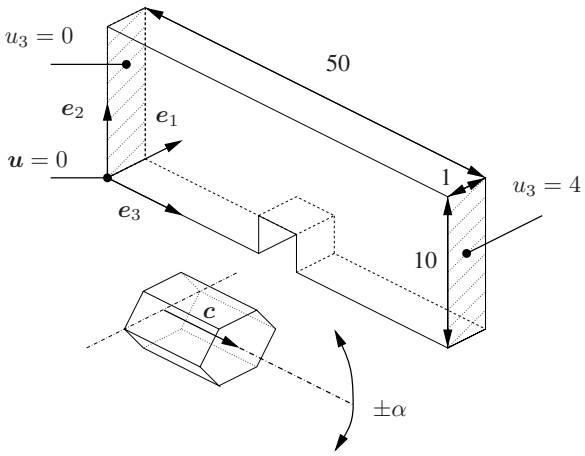

Fig. 15 Model of a notched band ($1 \times 10 \times 50$).

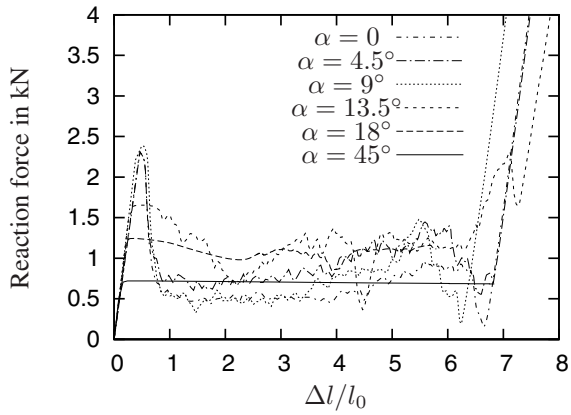

Fig. 16 Reaction force over the nominal elongation strain for the monotonic elongation of the band using the wedge-mesh with quadratic shape functions and taking into account basal slip, $\gamma_{\text{twin}} = 0.05\gamma_0$. As α increases, basal slip is triggered instead of twinning. With $\tau_{\text{twin}} \approx 4\tau_{\text{basal}}$, the force necessary to elongate the band decreases. For $\alpha = 45°$, the elongation is entirely realized by basal slip.

3.4.2 Cyclic loading and general observations

A cyclic loading test has been employed in order to examine the detwinning characteristics and the effect of the phenomenological model adaption. After loading the strip as depicted in Fig. 15, the loading has been reversed. Basal slip is disabled in the first place as well.

The band behaves initially linear elastic. At a certain point, a twin nucleates at the notch, and propagates rapidly through the width of the specimen. With ongoing loading, it propagates along its thickness direction, i.e. the established interface moves through the sample. After the entire specimen is twinned, one observes again linear elastic behavior. As the deformation is reversed, the behavior is similar to the loading process. One observes linear elastic behavior until the twin (which has initially been the parent) invades the specimen, and the initial state is restored. With the phenomenological model adaption, one is able to limit the stress at which twinning takes place, which is depicted in Fig. 17. One important result is that the critical force at which the linear elastic stage ends is doubled as the critical twinning shear γ_{twin} is doubled, which suggests

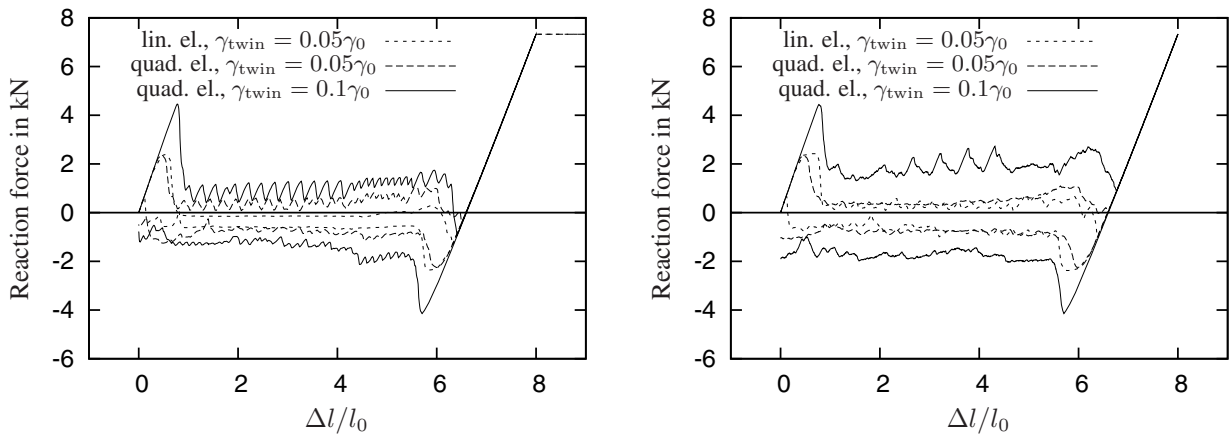

Fig. 17 Reaction force over the nominal elongation strain for the cyclic elongation, for regular meshes hexahedral meshes (left) and different wedge-meshes.

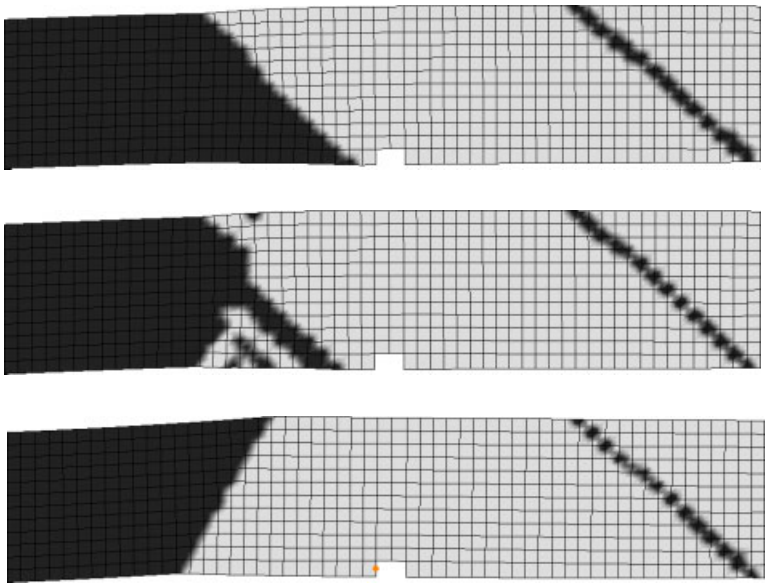

Fig. 18 The interface alignment shifts to the orientation of the conjugate twin.

that a proportional scaling $\tau_{\text{twin}} \approx G\gamma_{\text{twin}}$ can be used for stresses and strains of relevant order. The simulations with regular and irregular meshes yield approximately the same results.

One notes that the reaction force level is not constant in the stage of twin or parent propagation, irrespective of the jerky behavior. The reason herefore is that the stress state changes qualitatively during the loading. As the twin propagates, the band undergoes a shear deformation lateral to the elongation direction, which induces a small bending component. At load reversal, a slight necking is observed, causing again a small bending component. The change of the stress state is responsible for the sudden shifting of the interface, which has been observed in some calculations. Some exemplifying states are depicted in Fig. 18. The angle between the new and old interface is approximately $86°$, which means that we do not face a kink twin, but a pair of conjugate twins. The prediction of such behavior is a drawback of the elastic modeling. However, it is a minor problem in the primary loading stage, and only of matter if strain path changes occur on the twinned structure.

3.4.3 Distinction of conjugate twin systems

Due to the energy invariance of conjugate twin systems, it is interesting to see how they can be distinguished in an FE simulation. For this purpose, the phenomenological model adaption and basal slip have been deactivated. Therefore, the conjugate twin systems (the opposing twin systems in the hcp cell) are energetically not distinguishable (see Sect. 2.8). However, due to the asymmetry coming from the inclination of the crystal lattice with respect to the elongation direction, it has to be presumed that one twin system is preferred. In fact, one can clearly distinguish the twin bands that evolve, not by looking at both weight factors a_i or the strain energies w_i of the conjugate twin systems at a material point, but by relating the interface that evolves to the crystal basis. The conjugate twin systems can be triggered by inclining $\boldsymbol{c}$ by a small positive or a negative α, see Figs. 15 and 19. Inside the twin lamella the weight factors of the two equivalent twin systems are both approximately 0.5. The interface alignment clearly determines which of the conjugate twins has evolved, while the weight

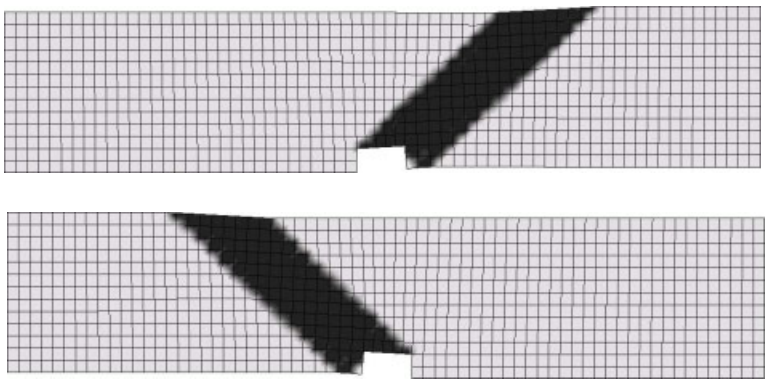

Fig. 19 Plot of the weight factor a_0 of the parent, $0(\text{black}) < a_0 < 1(\text{white})$, for a positive and negative inclination of the lattice with respect to the elongation direction.

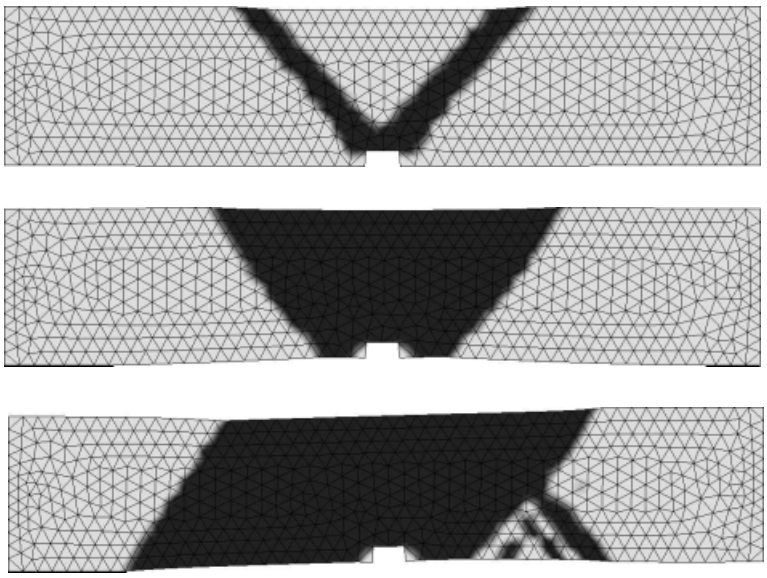

Fig. 20 Plot of the weight factor a_0 of the parent, $0(\text{black}) < a_0 < 1(\text{white})$. The elastic modeling induces artificial deformation modes, namely the interface shifting between conjugate twins and the union of conjugate twins.

factors are equal for any deformation. In fact, by canceling out one of the two conjugate twin systems in each of the three pairs, the FE calculation is not altered at all. Thus, the conjugate twin systems can be treated as one twinning mode.

One problem with the conjugate twin systems is that one twin may be bounded by interfaces belonging to the two distinct conjugate twins, as depicted in Fig. 20. The simulation has been carried out at a ten times larger elongation rate. It is observed that two regular conjugate twins unite to a mixed twin, which is an artifact of the model. The mixed twin is at least unstable and shifts quite fast to a regular twin.

In one case, a rather unexpected result has been encountered, namely the force displacement curve for the regular mesh with linear shape functions. In this simulation, the reaction force is not jerky, and in the first propagation stage it is negative, see Fig. 17. The implications of this are that the twin grows by itself, exerting a compressive force to the band, which contradicts physical experience. An explanation for this may be that an unfortunate combination of model parameters has been chosen. This suspicion is furnished by the fact that in no other simulation with a qualitative better FE model such behavior is observed.

3.4.4 Incorporation of basal glide

In this section, the twin-basal glide interaction is studied. The critical shear stress for basal glide is determined such that $\tau_{\text{twin}}/\tau_{\text{slip}} \approx 4$ holds. With $\gamma_{\text{twin}} = 0.05\gamma_0$, yielding $\tau_{\text{twin}} \approx 110$ MPa, $\tau_{\text{slip}} = 30$ MPa has been chosen. These values are larger than the values for pure magnesium, but reasonable for MgAl alloys. The elongation test has been carried out at $\alpha = 0, 4.5°, 9°, 13.5°, 18°$, and $45°$.

As expected, the basal slip activity depends on the inclination of the lattice. The simulation at $\alpha = 0°$ is practically unaffected by the incorporation of basal slip, though the basal plane is perpendicular to the tension direction. While the

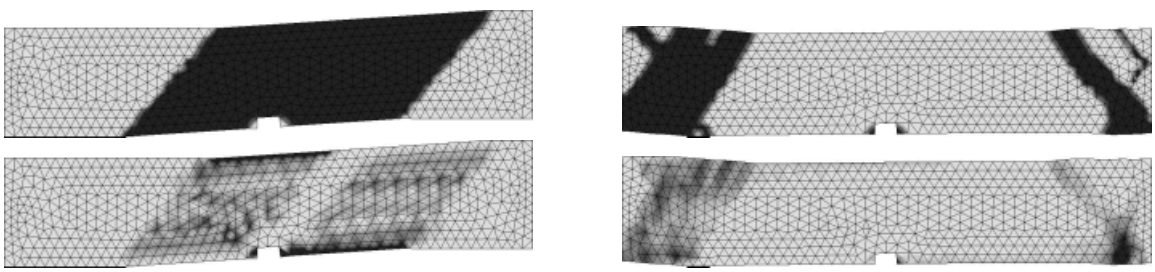

Fig. 21 Twin and basal slip evolution for the elongation test with $\alpha = 0°$. Above: Plot of the weight factor a_0 of the parent, $0(\text{black}) < a_0 < 1(\text{white})$. Below: Plot of the accumulated basal shear strain, from 0...0.025 in the left and 0...0.2 in the right figure. At the loading stage, the twin grows homogeneously into the parent, accompanied by slight basal slip. At the end of the loading stage basal slip is enforced at the band ends, which leads at load reversal to a heterogeneous twin structure (right).

twin nucleates and propagates, marginal slip activity is observed near the twin interface. As the twin interfaces reach the ends of the bar, more slip system activity is observed due to the fact that the boundary conditions at the ends of the band are incompatible with the twinning shear. The increased slip induces a less homogeneous parent structure, which triggers the evolution of a twin network at load reversal (Fig. 21).

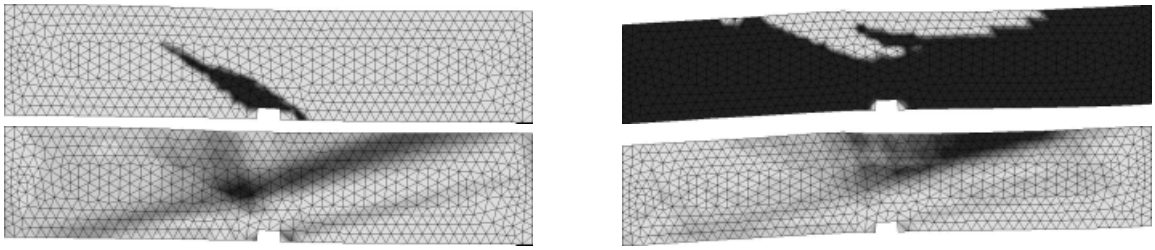

Fig. 22 Twin and basal slip evolution for the elongation test with $\alpha = 13.5°$. Above: Plot of the weight factor a_0 of the parent, $0(\text{black}) < a_0 < 1(\text{white})$. Below: Plot of the accumulated basal shear strain, from 0...0.15 in the left and 0...0.4 in the right figure. Note the cusp shape of the twin tip and the slip activity near the twin tip. The slip zone stretches to a slip band, which acts later as a boundary for twin growth.

For $\alpha = 4.5°$ and $\alpha = 9°$, similar behavior with more pronounced slip activity is observed. For $\alpha = 13.5°$, slipping and twinning interact already in the loading stage. Soon after the twin nucleates, a considerable amount of slip occurs near the twin tip (Fig. 22). Moreover, the twin tip has a pronounced cusp shape, as often observed in real crystals, and predicted by the theory of transformation dislocations (Boyko [15]). A slip band propagates at an angle of approximately $17.5°$ to the elongation direction, which is approximately parallel to the $\boldsymbol{c}$-axis. From this band, a distinguished zone of large slip deformation evolves, which acts as a barrier for the twin propagation (Fig. 22). Again, the major problem with the elastic modeling of twinning becomes visible. In the upper left subfigure in Fig. 22 one sees that the band undergoes a downward lateral deformation. In the final stage, the lateral shearing is upward. This means that the twin must have changed to its conjugate between the two states.

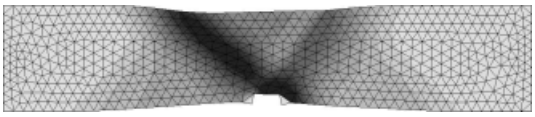

Fig. 23 Plot of the accumulated basal shear strain from 0...0.5, at $\alpha = 45°$. The entire elongation is accommodated by a slip band, and no twinning is observed.

In case of $\alpha = 45°$, slip bands evolve, and the deformation is entirely accommodated by basal slip, and no twinning is observed, Fig. 23. The critical force is approximately one fourth of the critical force in case of $\alpha = 0$, i.e., one recovers the ratio $\tau_{\text{twin}} \approx 4\tau_{\text{basal}}$.

The model setup is appropriate for further investigations, e.g., whether slip and twin interaction produce accommodation kinking. For magnesium, kink patterns are well documented by Roberts ([47]). It is found that two $\{10\bar{1}2\}$ twins that grow from the surface and meet inside the crystal enclose a triangle, in which accommodation kinking by a certain slip pattern is observed. This somewhat specific twin-slip-pattern can be reproduced successfully in a FE Simulation, see Fig. 24. The regular quadratic mesh has been used, with $\tau_{\text{twin}} \approx 110$ MPa, $\tau_{\text{basal}} = 30$ MPa, and $\alpha = 0$.

3.5 FE Model 3: Simple shear of a plane

3.5.1 Model setup

While the latter FE simulations resulted in approximately homogeneously loaded parts of twin and parent, in this section the effect of inhomogeneous loading conditions is examined. For this purpose, a 200 mm $\times$ 100 mm plane is subjected to a simple shear deformation, and the lattice is aligned such that the twin interfaces disturb the section-wise homogeneous deformation, unlike to the simulations of the two latter sections, see Fig. 25. Again, the deformation is restricted to be plane. One of the short edges is kept fixed while the opposing one is displaced proportional by 20 mm parallel to the fixed one. Loading occurs time proportional in 1000 s. If the lattice is oriented such that a rotation of $180°$ inside the is element of the symmetry group of the lattice, the model is point-symmetric with respect to the plane center point. The lattice is oriented such that the shear direction is parallel to $\boldsymbol{c}$ while the plane normal coincides with one of the $\boldsymbol{a}_i$. Therefore, only one half of the model has been incorporated, namely a 100 mm $\times$ 100 mm sheet, where the midpoint of one edge is fixed, while the opposing face is displaced 10 mm parallel the fixed edge. Along the fixed edge, $\boldsymbol{u}(d) = -\boldsymbol{u}(-d)$ holds, where

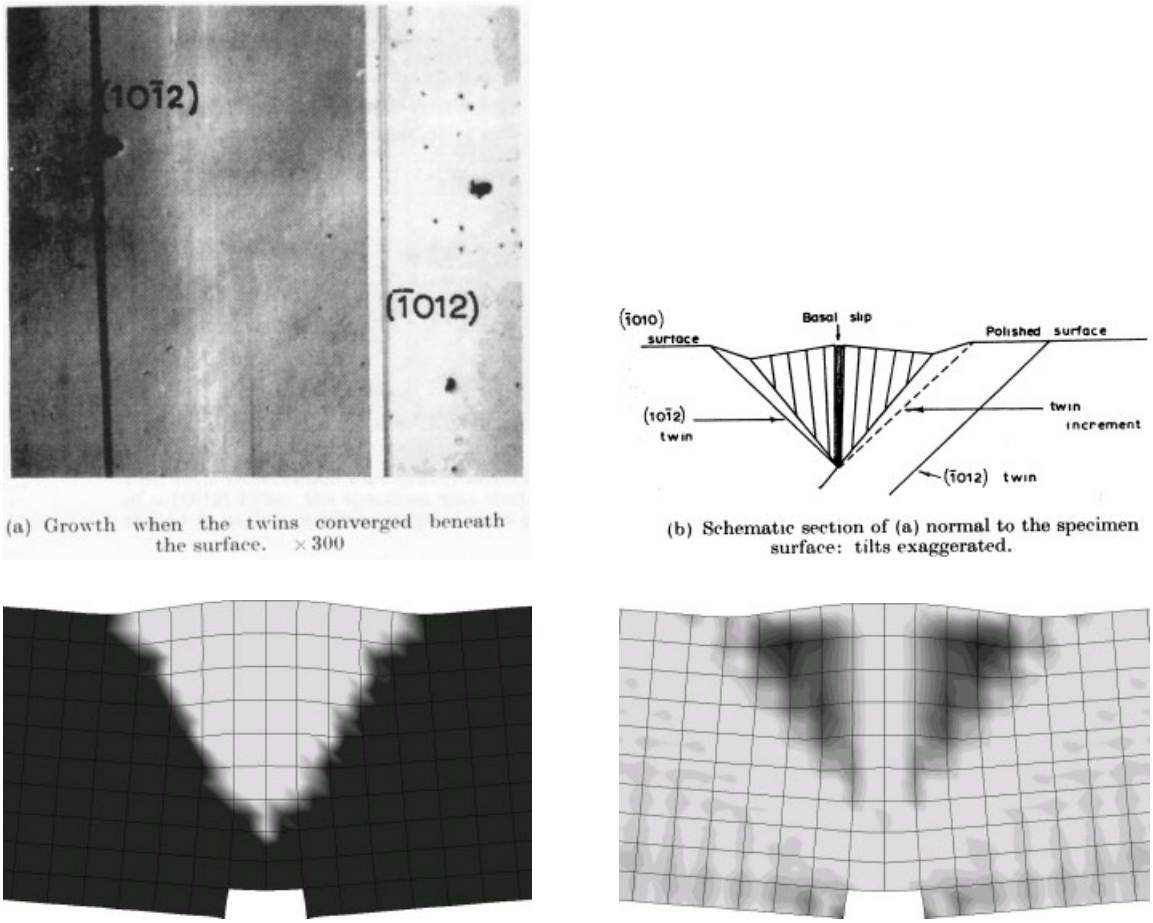

(a) Growth when the twins converged beneath the surface. ×300

(b) Schematic section of (a) normal to the specimen surface: tilts exaggerated.

Fig. 24 Kink pattern observed by Roberts [47] and simulated kink pattern. The deformation is scaled by a factor of 2 in order to magnify the kinks. Left: Plot of the weight factor a_0 of the parent, $0(\text{black}) < a_0 < 1(\text{white})$. Right: Plot of the accumulated basal shear strain, from 0...0.08.

d runs from -50 mm to 50 mm, see Fig. 25. A regular 50×50 mesh with quadratic elements (element type C3D20) has been used. Again, the regular mesh is regarded as unproblematic in this simulation, since the mesh interfaces intersect the twin interface at an angle of approximately $45°$.

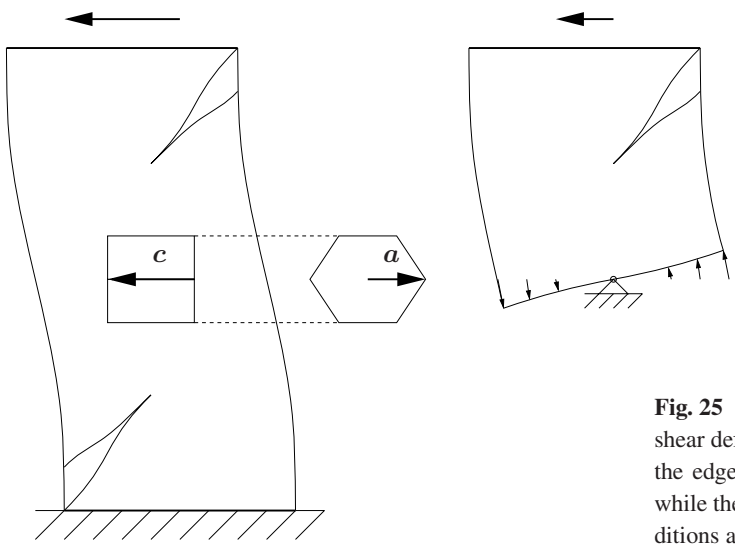

Fig. 25 Model of a plane (200×100) that is subjected to a simple shear deformation. The hexagonal crystal lattice is aligned such that the edge of the base hexagon is perpendicular to the model plane while the $\boldsymbol{c}$-axis is parallel to the shear direction. The boundary conditions are such that the deformation is plane.

3.5.2 Simulation results without basal slip

In the simulations, a twin nucleates in one corner and propagates fastly diagonally halfway through the plate. Then, as the loading continues, it grows thicker at the nucleation site while the tip of the twin remains sharp. Consequently, a cusp-shaped twin develops, with its interfaces slightly inclined to the $\{10\bar{1}2\}$ shear plane. However, the interfaces cannot be inclined beyond a certain angle, which depends on the twinning stress. After reaching the critical inclination, the twin breaks up into several twins, see Fig. 26. In Fig. 27, the twin shape just before the splitting of the twin is depicted for different twinning stresses. One notes that the larger the twinning stress is, the larger is the maximum interface inclination. This result is in agreement with analytical findings by Glüge [24]. Moreover, the cusp-shape of a twinning tip is predicted by the considerations regarding the dislocation nature of twinning (Boyko [15]), and observed experimentally as well, see Fig. 28.

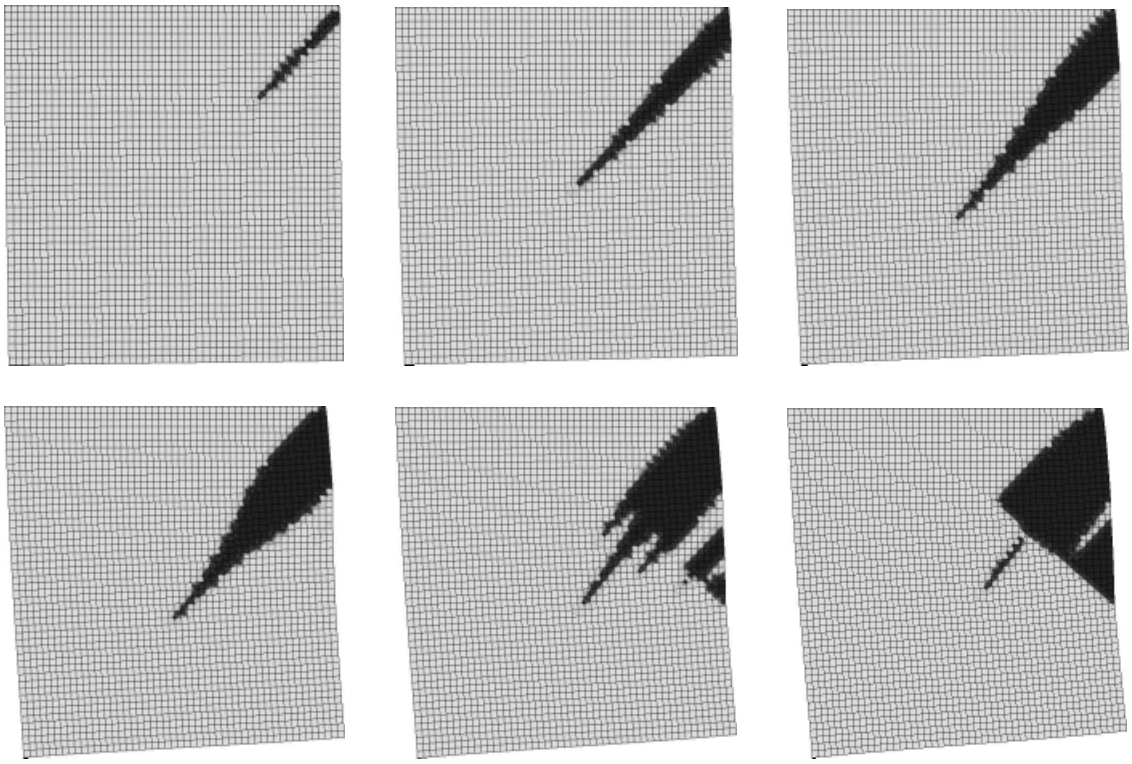

Fig. 26 Twin growth and breakup for $\tau_{\mathrm{twin}} \approx 240$ MPa, model depicted at 143 s, 283 s, 432 s, 605 s, 695 s and 800 s. Plot of the weight factor a_0 of the parent, $0(\mathrm{black}) < a_0 < 1(\mathrm{white})$.

3.5.3 Incorporation of basal glide

If basal slip is incorporated, the single-crystal simulations are very sensitive with respect to the initial conditions. At $\tau_{\mathrm{basal}} =$ 30 MPa and $\tau_{\mathrm{twin}} = 120$ MPa, a very small twin evolves (≈ 3 elements long), while the deformation is accommodated by basal slip in the large. If the lattice is rotated slightly (9° around the plane normal), the twin invades the plane, and the slip-twin interaction at the twin tip can be studied, see Fig. 29. One notes that the cusp-shape of the twin is practically lost. The reason for this is that basal slip accompanies the advancing twin tip, as the twin grows along the $\{10\bar{1}2\}$ shear plane. It appears that the slipping relaxes the stress state such that no large interface inclination is reached. Another interaction mechanism may be that the lattice is slightly rotated by the basal slip, possibly leaving it in an orientation more convenient for twin growth. Due to prior basal slip, one notes an overlapping of the zones of basal slip and the twin in Fig. 29.

4 Summary

The model that is presented here consists in its core of the quadratic St. Venant-Kirchhoff strain energy. It is extended by the isomorphy of the elastic law [11] and the Ball and James-approach [7] to a piecewise quadratic nonconvex elastic energy. To obtain a continuous differentiable strain energy, a regularization for the latter is introduced. Further, to adjust the

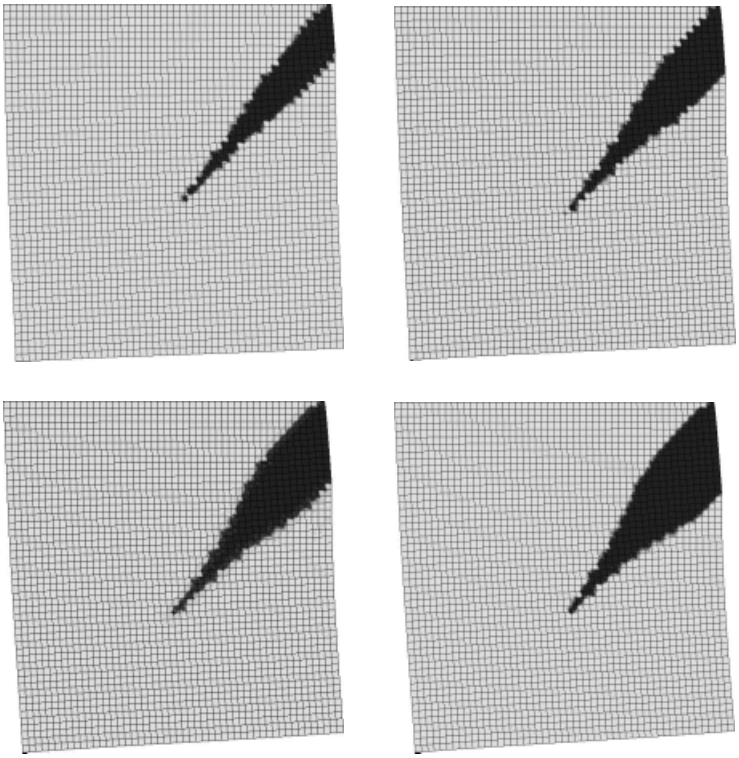

Fig. 27 Twins shortly before breakup for a twinning stress of 60 MPa (387 s), 120 MPa (484 s), 240 MPa (605 s) and 360 MPa (658 s). Plot of the weight factor a_0 of the parent, $0(\text{black}) < a_0 < 1(\text{white})$.

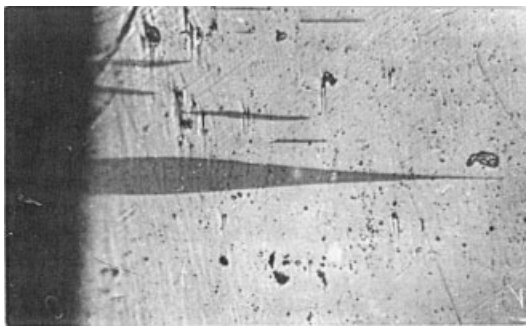

Fig. 28 Real twins may exhibit a cusp-shaped twin tip (bismuth single crystal, courtesy of Boyko [15]).

twinning-stresses, a phenomenological model adaption is introduced. In order to avoid the ill-posedness of the pseudoelastic boundary value problem, a viscous regularization is used. The model is applied to the $\{10\bar{1}2\}\langle\bar{1}011\rangle$ twinning in the hcp lattice, the twinning stress and the c/a ratio are close to common magnesium alloys. As hcp crystals undergo readily crystallographic glide in the basal plane, the fully viscoelastic model is extended by the card glide mechanism, which allows plastic deformations by basal slip in the parent crystal.

The model is tested in various finite element simulations. It is able to predict the nucleation and propagation of the twins. The stress-drop observed shortly after the nucleation (Christian [17]) and predicted by Kochmann [35] is found in the simulations as well. The predicted cusp-shape of the twin tips are in accordance with experimental findings and conclusions from the theory of transformation dislocations (Boyko [15]). Moreover, it is found that the interface inclination with respect to the shear plane is limited by the critical twinning stress, which is concluded from a stress jump analysis as well (Glüge [24]). In conjunction with the basal slip mechanism, the model is able to predict the kink patterns observed by Roberts [47].

However, the elastic modelling induces some difficulties. The most problematic fact is that twinning is connected to the movement of partial dislocations. This induces a strain path dependence and energy dissipation, which are neglected by any elastic modelling. Moreover, it can be shown that compound twins exhibit an elastic strain energy invariance, which connects each twin with its conjugate twin, and one is forced to deal with each pair of conjugate twins as one twinning mode. Practically all twins of practical interest are compound twins. If the conjugate twins are crystallographically equivalent, which is the case for many twinning modes in highly symmetric lattices, the strain energy invariance connects equivalent twin systems. It is shown that in that case, the conjugate twins can be distinguished clearly in the FE simulations by considering the interface orientation that evolves, but not the state of an individual material point. If the conjugate

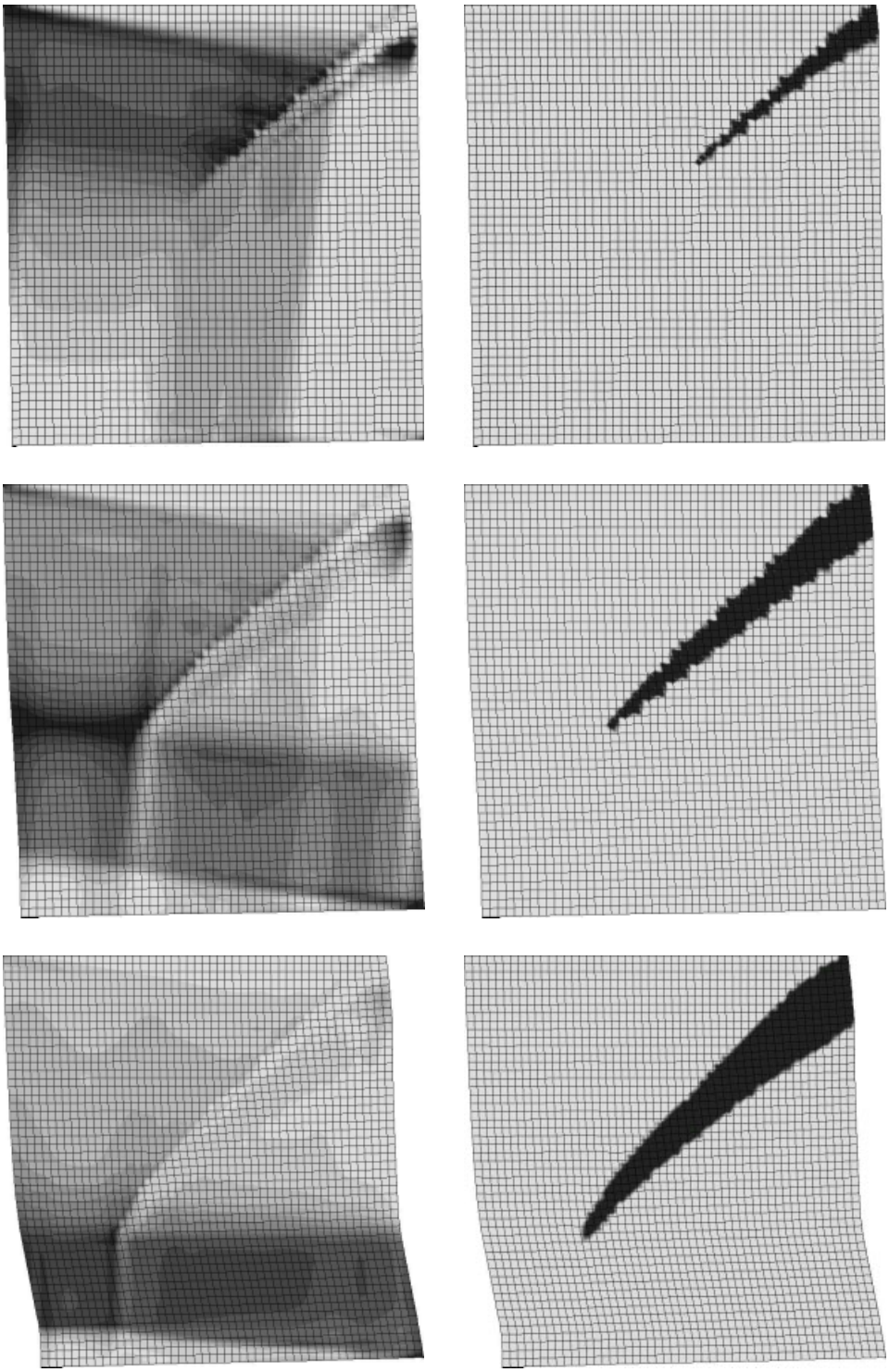

Fig. 29 Slip-twin interaction at the tip of the twin, $\tau_{\mathrm{twin}} = 120$ MPa, $\tau_{\mathrm{basal}} = 30$ MPa, states depicted at 223 s, 443 s, and 1000 s (from top to bottom row). Left: accumulated basal shear strain, 0...0.0375 (top), 0...0.075 (center) and 0...0.25 (bottom). Right: Plot of the weight factor a_0 of the parent, $0(\mathrm{black}) < a_0 < 1(\mathrm{white})$.

twins are crystallographically distinct, the elastic modelling cannot be applied, though crystallographically distinct twin systems would be treated as one twinning mode, regardles of their different physical properties. Another drawback which is intrinsical to the elastic modelling is that a fully developed twin may turn into another twin as the loading changes, which leaves to conclude that the elastic modelling is not suitable if severe strain path changes occur.

References

[1] R. Abeyaratne and J. Knowles, Evolution of Phase Transitions – A Continuum Theory (Cambridge University Press, Cambridge, 2006).

[2] E. Acerbi, G. Bouchitté, and I. Fonseca, Relaxation of convex functionals: The gap problem, Annales de l' Institut Henri Poincaré (C) Analyse non linéaire **20**, 359–390 (2003).

[3] G. Andrews, On the existence of solutions of the equation $u_{tt} = u_{xxt} + \sigma(u_x)_x$, J. Differ. Equ. **35**, 200–231 (1980).

[4] G. Andrews and J. Ball, Asymptotic behaviour and changes of phase in one-dimensional nonlinear viscoelasticity, J Differ. Equ. **44**, 306–341 (1982).

[5] R. Asaro and A. Needleman, Overview 42: Texture development and strain-hardening in rate dependent polycrystals, Acta Metall. **33**, 923–953 (1985).

[6] A. Atai and D. Steigmann, Coupled deformations of elastic curves and surfaces, Int. J. Solids Struct. **35**, 1915–1952 (1998).

[7] J. Ball and R. James, Fine phase mixtures as minimizers of energy, Arch. Ration. Mech. Anal. **100**, 13–52 (1987).

[8] J. Ball and R. James, Proposed experimental tests of a theory of fine microstructure, and the two-well problem, Philos. Trans. R. Soc. Lond. A **338**, 389–450 (1992).

[9] J. Ball, Convexity conditions and existence theorems in nonlinear elasticity, Arch. Ration. Mech. Anal. **63**, 337–403 (1977).

[10] J. Ball, P. Holmes, R. James, R. Pego, and P. Swart, On the dynamics of fine structure, J. Nonlinear Sci. **1**, 17–90 (1991).

[11] A. Bertram, Elasticity and Plasticity of Large Deformations (Springer Verlag, Berlin, 2005).

[12] T. Böhlke, The Voigt bound of the stress potential of isotropic viscoplastic FCC polycrystals, Arch. Mech. **56**, 423–443 (2004).

[13] T. Böhlke and A. Bertram, The evolution of Hooke's law due to texture development in polycrystals, Int. J. Solids Struct. **38**, 9437–9459 (2001).

[14] G. Bolling and R. Richman, Continual mechanical twinning, Parts I, II, III Acta Metall. **13**, 709–757 (1965); Continual mechanical twinning, Parts IV, V, Acta Metall. **14**, 637–647 (1965).

[15] V. Boyko, R. Garber, and A. Kossevich, Reversible Crystal Plasticity (AIP Press, New York, 1994).

[16] R. Cahn, Plastic deformation of alpha-uranium: twinning and slip, Acta Metall. **53**, 49–70 (1953).

[17] J. Christian and S. Mahajan, Deformation twinning, Prog. Mater. Sci. **39**, 1–157 (1995).

[18] C. Collins, Computation of twinning, The IMA Volumes in Mathematics and its Applications Vol. 54, (Springer, Berlin, Heidelberg, New York, 1993), pp. 39–50.

[19] C. Dafermos, The mixed initial-boundary value problem for the equations of nonlinear one-dimensional viscoelasticity, J. Differ. Equ. **6**, 71–86 (1969).

[20] E. Emles, Principles of Magnesium Technology (Pergamon, Oxford, 1966).

[21] J. Ericksen, Equilibrium of bars, J. Elast. **5**, 191–202 (1975).

[22] J. Ericksen, The Cauchy-Born hypothesis for crystals, in: Phase Transformations and Material Instabilities in Solids, edited by M. Gurtin (Academic Press, New York, 1984), pp. 61–77.

[23] J. Ericksen, Twinning of Crystals, IMA Preprint Series Univ. Minnesota **95**, 1–18 (1984).

[24] R. Glüge and J. Kalisch, A Lower Bound Estimation of a Twinning Stress for Mg by a Stress Jump Analysis at the Twin-parent Interface, in: Micro-Macro-Interactions in Structured Media and Particle Systems, edited by A. Bertram and J. Tomas (Springer-Verlag, Berlin, Heidelberg, New York, 2008).

[25] S. Govindjee, A. Mielke, and G. Hall, The free energy of mixing for n-variant martensitic phase transformations using quasi-convex analysis, J. Mech. Phys. Solids **51**, 1–26 (2003).

[26] M. Greenberg, On the existence, uniqueness, and stability of the equation $\rho_0 x_{tt} = e(x_x)x_{xx} + \lambda x_{xxt}$, J. Math. Anal. Appl. **25**, 575–591 (1969).

[27] M. Greenberg and R. MacCamy, On the exponential stability of solutions of $e(u_x)u_{xx} + \lambda u_{xtx} = \rho u_{tt}$, J. Math. Anal. Appl. **31**, 406–417 (1970).

[28] M. Greenberg, R. MacCamy, and V. Mizel, On the existence, uniqueness, and stability of solutions of the equation $\sigma'(u_x)u_{xx} + \lambda u_{xtx} = \rho_0 u_{tt}$, J. Appl. Math. Mech. **17**, 707–728 (1968).

[29] P. Haasen, Physical Metallurgy, 3rd edition (Cambridge University Press, Cambridge, 1996).

[30] R. Hill, On constitutive inequalities for simple materials-I, J. Mech. Phys. Solids **16**, 229–242 (1968).

[31] Q. Hu, L. Li, and N. Ghoneim, Stick-slip dynamics of coherent twin boundaries in copper, Acta Mater. **57**, 4866–4873 (2009).

[32] J. Hutchinson, Bounds and self-consistent estimates for creep of polycrystalline materials, Proc. R. Soc. Lond. A **348**, 101–127 (1976).

[33] K. Kawabata, Y. Hosokawa, T. Saga, and T. Sambongi, Real-time observation of twin boundary motion in crystals: an ideal dry friction system, Tribology Letters **9**, 41–44 (2000).

[34] P. Klouček and M. Luskin, The computation of the dynmaics of the martensitic transformation, Contin. Mech. Thermodyn. **6**, 209–240 (1994).

[35] D. Kochmann and K. Le, A continuum model for initiation and evolution of deformation twinning, J. Mech. Phys. Solids **57**, 987–1002 (2009).

[36] M. Lambrecht, C. Miehe, and J. Dettmar, Energy relaxation of non-convex incremental stress potentials in a strain-softening elastic-plastic bar, Int. J. Solids Struct. **40**, 1369–1391 (2003).

[37] B. Li and E. Ma, Atomic shuffling dominated mechanism for deformation twinning in magnesium, Phys. Rev. Lett. **103**, 35503-1-4 (2009).

[38] B. Li and E. Ma, Zonal dislocations mediating $\{1011\}\langle 1012\rangle$ twinning in magnesium, Acta Mater. **57**, 1734–1743 (2009).

[39] S. Lubenets, V. Startsev, and L. Fomenko, Elastic Twinning in In-10 Wt% Pb Alloy, Krist. Tech. **15**, K78–K80 (1980).

[40] I. Müller and P. Villaggio, A model for an elastic-plastic body, Arch. Ration. Mech. Anal. **65**, 25–46 (1977).

[41] P. Neumann, Vereinfachung kristallographischer Rechnungen in hexagonalen Gittern durch konsequente Benutzung des vierachsigen hexagonalen Koordinatensystems, phys. stat. sol. **17**, K71–K74 (1966).
[42] M. Ortiz and E. Repetto, Nonconvex energy minimization and dislocation structures in ductile single crystals, J. Mech. Phys. Solids **47**, 397–462 (1999).
[43] S. Pagano and P. Alart, Solid-solid phase transition modelling: relaxation procedures, configurational energies and thermomechanical behaviours, Int. J. Eng. Sci. **37**, 1821–1840 (1999).
[44] R. Pego, Phase transitions in one-dimensional nonlinear viscoelasticity: Admissibility and stability, Arch. Ration. Mech. Anal. **97**, 353–394 (1987).
[45] M. Peigney, A non-convex lower bound on the effective energy of polycrystalline shape memory alloys, J. Mech. Phys. Solids **57**, 970–986 (2009).
[46] M. Pitteri and G. Zanzotto, Continuum Models for Phase Transitions and Twinning in Crystals (Chapman and Hall/CRC, London, 2002).
[47] E. Roberts and P. Partridge, The accommodation around $\{10\bar{1}2\}\langle\bar{1}011\rangle$ twins in magnesium, Acta Metall. **14**, 513–527 (1966).
[48] B. Schmidt, Linear Γ-limits of multiwell energies in nonlinear elasticity theory, Contin. Mech. Thermodyn. **20**, 375–396 (2008).
[49] M. Shiekhelsouk, V. Favier, K. Inal, and M. Cherkaoui, Modelling the behaviour of polycrystalline austenitic steel with twinning-induced plasticity effect, Int. J. Plast. **25**, 105–133 (2009).
[50] M. Sidi Ammi and D. Torres, Regularity of Solutins of the Autonomous Integrals of the Calculus of Variations, in: Differential Equations, Chaos and Variational Problems, (Springer, Berlin, Heidelberg, New York, 2008).
[51] S. Silling, Phase changes induced by deformation in isothermal elastic crystals, J. Mech. Phys. Solids **37**, 293–316 (1989).
[52] G. Simmons and H. Wang, Single Crystal Elastic Constants and Calculated Aggregate Properties: A Handbook (The MIT Press, Cambridge, MA, 1971).
[53] J. Simo and T. Hughes, Computational Inelasticity (Springer-Verlag, New York, 1998).
[54] J. Stark, Mechanical twinning in crystals, Phys. Rev, B **38**, 1139–1142 (1988).
[55] P. Swart and P. Homes, Energy minimization and the formation of microstructure in dynamic antiplane shear, Arch. Ration. Mech. Anal. **121**, 37–85 (1992).
[56] C. A. Truesdell and W. Noll, The Non-linear Field Theories of Mechanics, in: Encyclopedia of Physics, Vol. III/3 (Springer, Berlin, 1965).
[57] Y. Wang, Y. Jin, and A. Khachaturyan, The Effects of Free Surfaces on Martensite Microstructures: 3D Phase Field Microelasticity Simulation Study, Acta Mater. **52**(4), 1039–1050 (2004).
[58] G. Zanzotto, On the material symmetry group of elastic crystals and the Born rule, Arch. Ration. Mech. Anal. **121**, 1–36 (1992).
[59] G. Zanzotto, The Cauchy-Born hypothesis, nNonlinear elasticity and mechanical twinning in crystals, Acta Crystallogr. A **52**, 839–849 (1996).

